Title
THE PHOTOPRODUCTION OF MESONS FROM HYDROGEN

Author
Bishop, A.S.

Publication Date
1950-08-24

UNIVERSITY OF CALIFORNIA

Radiation Laboratory

BERKELEY, CALIFORNIA

DISCLAIMER

UCRL 874

UCRL 874

The Photoproduction of Mesons from Hydrogen (Aug 1950)

by

Amasa Stone Bishop
B.S. (California Institute of Technology) 1943

DISSERTATION

Submitted in partial satisfaction of the requirements for the degree of

DOCTOR OF PHILOSOPHY

in

Physics

in the

GRADUATE DIVISION

of the

UNIVERSITY OF CALIFORNIA

Approved:

. . . . . .

. . . . . .

. . . . . .

. . . . . .

Committee in Charge

Deposited in the University Library . . . . . .
Date Librarian

The Photoproduction of Mesons from Hydrogen

by

Amasa Stone Bishop

TABLE OF CONTENTS

TABLE OF CONTENTS (Cont.)

I ABSTRACT

In an effort to gain information on the nature of the photon-meson and photon-nucleon interaction, a study of the artificial production of mesons by photons has been made at the Berkeley synchrotron. The major effort of this research was concentrated on a measurement of the energy and angular distribution of π^+-mesons produced when the photons strike a target of liquid hydrogen. Detection of the mesons is accomplished electronically by the technique of delayed coincidence.

Since the photons are completely absorbed in the process of meson creation ($\gamma + p \longrightarrow n + \pi^+$), conservation of energy and momentum requires that, for a given angle of emission of meson, there be an exact relationship between the energy of the meson and the energy of the photon responsible for its creation. Thus, from the measured energy distribution of the mesons at 90° (see Fig. 15), and the theoretical energy distribution of the photons from the synchrotron, it is possible to determine the excitation function (Fig. 16) for photoproduction of mesons at 90°.

This excitation function is seen to increase rather slowly from threshold and to flatten off somewhat with increasing photon energy. Modification of the data which may be required as a result of nuclear absorption is indicated.

The angular distribution of mesons was measured for a single photon energy of 250 Mev, the absorber thickness being varied with the angle of measurement. This distribution, plotted in Fig. 19 as a function of angle in the center of mass system, is seen to be roughly isotropic but

peaked slightly in the backward direction.

Included in this report is an outline of the several meson theories which have been developed to date, together with graphs of the energy and angular distributions of photomesons which would be predicted on the basis of some of these theories. The experimental data are then compared with the results of these various theories.

Such a comparison provides evidence that π^+-mesons have zero spin and that they are tightly coupled to nucleons. These properties are consistent with the pseudoscalar meson theory. It must be stressed, however, that at the present time no meson theory is completely free of experimental contradictions or theoretical complications, and hence these results cannot be said to be a striking confirmation of any meson theory yet developed. Rather it seems probable that a revision of the basic formulation of meson theory is necessarily in the offing.

II INTRODUCTION

A. History and Background

Ever since mesons were predicted by Yukawa in 1935 and subsequently discovered by Anderson in cosmic rays in 1937, a vast amount of theoretical and experimental effort has been expended upon the study of these particles and the force fields associated with them. With the passage of time, additional types of mesons have been discovered and the entire interpretation of the role of mesons has become increasingly complicated, if not somewhat confused.

For a long time (1937 - 1948), the experimental study of mesons was confined to those produced in cosmic rays, and the consequent lack of controlled experiments resulted in a slow accumulation of experimental data. Progress was further hindered by the fact that no accurate or quantitative predictions could be made. Even up to the present time no general theory of fundamental particles has been developed which is capable of predicting even such basic characteristics as mass or spin, to say nothing of such involved properties as interaction with other particles. In addition, the generally accepted method of expressing the interaction between particles, that of formulating a quantized field theory of nuclear forces based on analogy with quantized electromagnetic field theory, has problems of divergences which appear to date to be much more serious in nuclear field theory than in quantum electrodynamics.

Present theories are based on the assumption that π-mesons (rather than the earlier discovered μ-mesons) constitute the quanta of the nuclear force field and are hence intimately related to nuclear forces. However, a knowledge of the types of interactions which exist between

fundamental particles, as well as the strength of these interactions, has been almost wholly lacking.

The experimental determination of such basic properties as mass and lifetime of mesons is essentially straightforward. The determination of the interactions between them and other fundamental particles is, however, a great deal more complicated, since the experimental data must be correlated with theory. Recently, artificial production of mesons by high energy nucleons[1] and by high energy x-rays[2] has made it possible to perform basic experiments, under controlled conditions, on the mode of interaction of mesons.

B. Photoproduction of Mesons; Energy and Angle of Emission

Probably the simplest* type of nuclear process which yields information on meson interaction is that of photoproduction of mesons from a single nucleon. (The presence of other nucleons within the target nucleus produces an interference in the production of mesons, severely complicating the experimental and theoretical results: see Section IV, B.) For this reason a study of the production of π^+-mesons by photons in hydrogen was undertaken, the source of photons being the 322 Mev Berkeley synchrotron. Initial experiments were performed by successively interchanging targets of polyethylene $(CH)^N$ and carbon, the hydrogen results being obtained by subtraction. Subsequent experiments were performed with liquid hydrogen as a target.

The process which is believed to occur is the interaction of a

---

* The production of mesons by proton-proton collision provides another fundamental source of studying meson interactions. However, the interpretation of the energy and angular distribution of the mesons[3] is complicated by the interaction between the resultant neutron and proton.

photon with a proton, with the subsequent emission of a π^+-meson and the conversion of the proton into a neutron. Symbolically,

$$\gamma + p \longrightarrow \pi^+ + n$$

Application of the equations of conservation of energy and momentum provide the following relationship (derived in Appendix A):

$$k = \frac{1.236 \times 10^5 + 938.7\ T_\pi}{797.7 - T_\pi + \cos\theta\ (T_\pi^2 + 282\ T_\pi)^{1/2}} \qquad (1)$$

where

k = photon energy in laboratory system in Mev

T_π = meson kinetic energy (laboratory system) in Mev

θ = angle of meson emission (laboratory system)

This relationship is plotted in Fig. 1 for several angles θ of meson emission. The energy threshold in the laboratory system for meson production, found by setting $T_\pi = 0$, is easily found to be 155 Mev. (In the center of mass system, the threshold is 152 Mev.)

C. Characteristics of π^+ and μ^+-mesons; Use of $\mu^+ - e^+$ Decay for Identification

The π^+-meson constitutes a particularly favorable species of meson on which to perform experiments, since it initiates a train of distinctive events which may be used for its identification. Because of its positive charge, a π^+-meson which has been brought to rest within matter is repelled by the Coulomb field of the surrounding nuclei, with the result that, unlike a π^--meson, its absorption by nuclei is very unlikely. Instead, it decays spontaneously with a mean-life of about 10^{-8} seconds[4] into a μ^+-meson (and a single neutral particle, probably a neutrino). The μ^+-meson is emitted with an energy of 4 Mev and has a range of about

0.2 grams/cm^2. Upon being brought to rest, it in turn decays with the well-known mean-life of 2.15×10^{-6} seconds[5] into a positive electron (and probably two neutrinos). The electron emitted in μ^+ decay has an upper energy limit of 56 Mev. Thus, the life history of the π^+-meson may be designated schematically as follows:

$$\pi^+ \xrightarrow{\sim 10^{-8}\ \text{s.}} \mu^+ \ (+\nu) \xrightarrow{2.15 \times 10^{-6}\ \text{s.}} e^+ \ (+2\nu)$$

Either one or both of these decays may be used in practice to provide a satisfactory means of electronic meson detection. At the time that this research was carried out, stable electronics capable of resolving the π^+-μ^+ decay interval were not available here and we contented ourselves with the μ^+-e^+ decay as a means of meson indentification.

D. Characteristics of Scintillation Counters; Reasons for Use

Scintillation counters have been used for a number of years for the detection of charged particles. Passage of any charged particle through the crystal causes excitation of the molecules within the crystal, and the subsequent electronic transitions back to the ground state result in the emission of light quanta. In the case of stilbene and anthracene, the transition to the ground state occurs in a time less than 10^{-7} seconds,* and hence these crystals may be used in conjunction with a phototube to resolve the pulses initiated by two particles separated by 10^{-7} seconds or more in time, as is required for the electronic identification of a π^+ meson by means of its decay electron.

The principal reason for using scintillation counters as against

---

* In stilbene the time is $\sim 8 \times 10^{-9}$ sec.

photographic plates is, of course, the rapidity with which mesons can be counted. With the usual synchrotron intensity of about 10^4 ergs/second, and the geometry used in these experiments (see Fig. 9, for example), the meson counting rate is about 15 counts/minute. Offsetting somewhat this advantage of high counting rates, however, is the fact that to date no reliable method has been developed for counting negative mesons with crystals. (This does not, however, constitute a disadvantage in this particular application, since it is not believed possible to produce negative mesons by photoproduction from hydrogen.)

III METHOD OF MESON DETECTION

A. The X-ray Beam

The location of the apparatus with respect to the synchrotron is shown in Fig. 2. Electrons are accelerated in the synchrotron to an energy of 322 ± 6 million electron volts and stike a 0.020 inch platinum target placed within the evacuated accelerating doughnut. The photons produced by bremsstrahlung in the target are emitted in a narrow cone which has a width (at half-intensity) of 0.77 degrees. A tapered hole in a block of lead placed 55 inches from the target serves to collimate the beam. In these experiments the entrance diameter of the collimator hole was usually selected to be one inch.

Behind the collimator, and as close to it as practicable, is situated the photon target, in which the mesons are created. In this region is also housed the meson detecting apparatus, embedded in heavy shielding, which serves to eliminate the major part of the radiation which envelopes the synchrotron during bombardment.

B. Method of Obtaining the Spread-out Beam

In usual synchrotron operation the radiofrequency accelerating voltage is cut off when the magnetic field is at its peak, and the electrons spiral inward to strike the target over a period of about 10 microseconds. For the purposes of meson counting, however, it is advantageous to spread the beam out over several thousand microseconds, since the background counting rate is inversely proportional to the duty cycle of the beam. This spread-out beam is best accomplished[6] by changing the shape of the r.f. pulse from a square wave form to one which approaches exponentially the voltage needed to barely sustain the electrons in the equilibrium

orbit. As early, then, as 10 degrees before peak magnetic field, the magnitude of the r.f. is not sufficient to prevent some of the electrons from spiraling into the target, with the result that the electrons strike the target over a period of several thousand microseconds, as shown in Fig. 3. The electrons striking the target have an associated spread in energy from 295 to 322 Mev.

C. Electronic Detection Technique

The identification of the mesons is accomplished by the method of delayed coincidences,[7] shown schematically in Fig. 4. Three crystals, with accompanying phototubes and amplifiers, are utilized. In order for an initiating particle to be counted electronically as a meson, we require that it lose more than 6 Mev in passing through the first crystal, that it stop in the second crystal with a release of more than 5 Mev, and that it give no pulse in the third. Thus, electronically, the first two crystals are connected in coincidence, and the output of this coincidence circuit is connected in anticoincidence with the third crystal. A particle which satisfies these requirements succeeds in initiating a series of four successive delayed "gates," each of about 2 microseconds duration. The first gate opens about 0.5 microseconds after the initiating pulse, remains open for 2 microseconds, and closes. Immediately the second gate opens, remains open for 2 microseconds, and closes, etc.

A π^+-meson from the target which stops in the second crystal will produce three successive pulses in this crystal: the first pulse constitutes the π^+-meson slowing down and coming to rest; the second pulse, about 10^{-8} microseconds later (and indistinguishable from the first as far as our electronics are concerned), constitutes the μ^+-meson being

emitted and being brought to rest; the third pulse, several microseconds later, corresponds to the emission of the decay electron.

Thus the pulse from a π^+-meson which has stopped in the second crystal (thereby initiating the set of four delayed gates) will be followed in a few microseconds by a pulse from the decay electron, again in the same second crystal. This pulse is then placed electronically in coincidence with each of the four delayed gates. Since the gates extend over the region of 0.5 to 8.5 microseconds after the initiating pulse, and since the half-life of the π^+-meson is 2.15 microseconds,[5] about 80 percent of the decay electrons will be "caught" in one or another of the delayed gates. Coincidences with these gates are registered on scalers and constitute an indication of the mesons counted. In addition, single counting rates of the crystals are also registered both as a matter of interest and as a means of background determination. (A typical data sheet, together with a definition of the notation, is given in Appendix B. A photograph of the electronic apparatus is given in Fig. 5, and the circuits are given in Appendix C.)

D. Background Determination

It is clear, however, that events other than the capture of a meson may be registed with the electronic apparatus described above. For example, an event such as the passage of a proton through the first crystal and stopping in the second, followed in a few microseconds by, say, an electron from the target or from the synchrotron, will satisfy all of the above requirements and will hence be registered as a meson. Such counts constitute "background," and must be subtracted off to give the real meson counts.

Two independent methods of determining the background counting

rate have been used in these experiments:

a) A measured gate of approximately 2 microseconds is delayed for an interval of 15 microseconds, at which time the number of delayed electrons originating from mesons will be negligible. If this gate is initiated each time the "meson" gates are initiated, and II_b pulses (i.e., low level pulses - mostly electrons - detected in crystal II) are set in coincidence with this gate, the number of coincidences registered will constitute essentially pure background.*

b) The second method is to compute the number of random coincidences which would be expected. In a time interval T, the total time a meson gate is opened is given by $G\Delta$, where Δ is the gate width, and G is the number of gates initiated in time T. If there are II_b "electron" counts in time T placed randomly in coincidence with these gates, the number of coincidence counts in T is

$$N_{background} = \frac{G\Delta II_b}{T \times \text{duty cycle}}$$

The duty cycle, i.e., the fraction of time that the x-ray beam exists, can be measured and remains constant to within 10 percent.

---

* Such a method of background determination will in general have rather large statistical errors due to the small background counting rate. A method of overcoming this difficulty is to increase artificially the number of gates by a known factor, and thereby decrease the statistical error of the coincidence counts. In practice, this long-delayed gate was initiated by single pulses (III) from the third crystal. The number of actual background counts is then given by:

$$N_{background} = (\text{no. of coincidences between gate and } II_b) \times \frac{G}{III},$$

where G = number of pulses from the output of the coincidence-anticoincidence circuit. (See Fig. 4.)

E. Corrections for Nuclear Absorption

In addition to background subtraction, the observed counting rates must be corrected for nuclear absorption.

Nuclear absorption is defined here to be the interaction between the mesons in flight and the atomic nuclei of the absorbers through which they pass, resulting either in absorption of the mesons or in wide angle scattering. The cross section for nuclear interaction for meson energies of <50 Mev is not yet accurately known and hence final corrections cannot be made at this time. However, the experimental work of Fowler et al.[8] indicate that in this energy region the cross section may be as great as the nuclear area. Such a large cross section will result in sizable corrections to the experimental data, since mesons which pass through a large amount of absorber will have a greater probability of nuclear interaction than those which pass through a small amount with such a cross section. Corrections have been computed for nuclear interactions with cross sections equal to nuclear area ($R = 1.38\ A^{1/3} \times 10^{-13}$ cm), and are shown in the final results.

F. Evidence of Meson Counting

The counting technique having been developed, one must convince oneself that, in truth, mesons are being detected rather than, for example, some other nuclear event which occurs with a comparable half-life to that of the meson. The following evidence is therefore presented as rather substantial proof that the equipment is detecting $\pi^+ \longrightarrow \mu^+ \longrightarrow e^+$ events.

a) The measured mean-life (see Appendix F) is equal to the accepted value of the μ^+-meson within experimental error.

b) Within experimental error, the measured upper limit of the energy (at a given angle) of the emitted particles agrees with

the theoretical value to be expected (from energy and momentum considerations) if the particles are π^+-mesons.

c) The measured energy and angular distribution from carbon agree, within experimental error, with those found by J. Peterson,[9] using photographic plates.

d) The measured energy distribution from hydrogen agrees, within experimental error, with the data of Cook,[10] who made preliminary measurements with photographic plates.

G. Determination of Discriminator Levels; Plateau Curves; Counting Efficiency

An important factor in counting mesons electronically is the proper setting of the discriminator levels of the various shaping circuits. These levels determine the minimum amount of energy which a particle must lose in the crystals if it is to be counted.

In order to set these discriminator levels intelligently, one must estimate the minimum energy loss to be expected in crystals I and II when a π^+-meson is brought to rest in crystal II. Since the μ^+-meson has such a short range, it will almost always lose its entire kinetic energy of 4.05 Mev in the second crystal. The additional amount of energy which the π^+-meson will lose in this same crystal will depend upon its depth of penetration before it is brought to rest. In any case, one should expect a total energy loss of more than 4 Mev when a π^+-meson stops in crystal II.

From range-energy relationships, it is easy to show that the minimum energy lost in crystal I (0.75 inch thick) by a π-meson passing all the way through crystal I and stopping in crystal II is about 6 Mev.

The discriminators of channels I and II_a should thus be set to

accept only pulses which correspond to energy losses in excess of these minimum values. The acceptance of smaller pulses would result in an increase of background (due to additional gates) without a corresponding increase in meson yield.

The discriminator setting for the delayed electron pulse (II_b) in crystal II must of course be separate from that for the meson pulse (II_a), since the energy loss by the electron in escaping from the crystal will in general be appreciably lower than 4 Mev. In setting this bias level one must select a value which will provide the optimum number of mesons without an excessive number of background counts.

As an aid in the setting of the proper discriminator levels, bombardments were made in which the number of mesons was determined as a function of the minimum accepted pulse height in channels I, II_a, and II_b. These "plateau curves" are shown in Figs. 6, 7 and 8 respectively. As would be expected, these curves show a definite plateau for the delayed coincidence (i.e., mesons) when the discriminator levels of channels I and II_a are varied, but little or no plateau for the II_b (electron) channel. Also indicated in these figures are the single counting rates, which, of course, increase rapidly as the discriminator level is lowered.

In order to achieve simultaneously good repeatability of data, a large number of mesons, and a low background, it is clear that the discriminator levels of channels I and II_a should be selected to lie at the high end of the plateau region, as indicated in the figures. In the case of the II_b channel, its setting is somewhat more arbitrary; to some extent it is dependent upon the intensity of the synchrotron beam. In view of the lack of a plateau, slow drifts in B+ and tube voltages in channel II could cause slow drifts in the delayed coincidence counting

rate. For this reason, the discriminator level was checked periodically throughout any bombardment by placing a radium source a given distance away from the crystal and adjusting the discriminator, when necessary, to give a predetermined counting rate of the single pulses.

These plateau curves serve also as an aid in estimating the efficiency of the crystals in counting mesons under a particular set of discriminator settings. They indicate, for example, that under the usual operating conditions the counting efficiency is approximately 50 percent.

IV METHOD OF CARBON-POLYETHYLENE SUBTRACTION

Since the method of subtraction was used primarily as a preliminary experiment, and since the results were in large part superseded by the later experiment with liquid hydrogen, the experimental procedure will only be outlined here and the results given mainly for comparison with the later data.

The experimental setup is shown in Fig. 9. Mesons produced at the target lose energy in the aluminum absorber and enter the scintillation crystals, where they are detected by the method described above. The aluminum channel was inserted to decrease the possibility of mesons scattered at small angles from the lead having sufficient energy to reach the crystals.

The cylindrical targets of carbon and polyethylene were successively interchanged during the bombardment in order to reduce the systematic errors caused by voltage drift of the electronic equipment.

In order that the two targets be of the same size and also that the energy loss of the mesons escaping from the target be identical, it was necessary to build the carbon target in cylindrical form out of thin laminations of carbon, with planes perpendicular to the direction of the crystals.

A. Energy Distribution

The energy distribution was measured simply by recording the number of mesons stopping in the crystal as a function of the thickness of the aluminum absorber; the meson energy is determined, of course, by range-energy relationships. Fig. 10 shows the relative number of mesons produced by carbon atoms and hydrogen atoms at 90° in the laboratory system,

as a function of the meson energy.[11] The incident photons have approximately a bremsstrahlung spectrum of 322 Mev maximum energy.* The carbon data agree, within statistical error, with the results of Peterson,[9] who used photographic plates to measure the energy distribution at 90° from carbon.

B. Effects of Nuclear Interference on Meson Production from Carbon

The most interesting, if not suprising, result of this measurement is that the cross section of the six bound protons in a carbon atom is only about twice as great as that of a single free proton. Such a result can only be caused by nuclear binding, and can, in fact, be interpreted as a consequence of the Pauli exclusion principle, since the recoil nucleons have energies not greatly in excess of the Fermi energy. A calculation of the effects of nuclear binding to be found in helium targets has been made by Chew and Lewis.[12] These computations show that in helium it is possible to account for a ratio σ (free proton)/ σ (bound proton) as large as three. Similar computations for carbon have not yet been made, but one would expect a similar ratio.

C. Angular Distribution

In the case of angular distribution, the measurement which can most easily be compared with theory is that in which a single photon energy is selected. Thus, a different thickness absorber was used at each of the five angles measured, such that those mesons produced from a free proton were created by 250 Mev photons. This photon energy was selected in view of the fact that, at 90°, the maximum of the energy

---

* For a detailed computation of the photon spectrum, see Section V, C.

distribution occurs roughly at this photon energy.

The various angles were obtained by rotating the detection apparatus about the target as an axis. The measured cross section,[11] as a function of angle in the center of mass system, is shown in Fig. 11 for both hydrogen and carbon. (For the carbon points, the analysis has been carried through in the same way as for the hydrogen, although there the binding of the nucleons makes the momentum and energy conservation arguments invalid.) While the cross sections have been plotted in absolute units, the error of the absolute value was known to be quite large, since the counting efficiency of the crystals had not been accurately determined at this time.

V ENERGY DISTRIBUTION AND EXCITATION FUNCTION FROM LIQUID HYDROGEN

A. Advantage of Using Hydrogen over the Subtraction Method

Preliminary data having been obtained by the method of subtraction, it was desirable to repeat the experiments with liquid hydrogen as the target. The advantages of obtaining results from hydrogen directly rather than by the subtraction method are the following:

a) because there is no subtraction, the statistical errors are much lower for the same number of mesons counted. For example, to obtain 5 percent statistics by direct production from hydrogen requires only 400 real meson counts (if background counts are neglected), whereas in the subtraction method, over 1000 real counts are needed.

b) With hydrogen as target the background from the target is lower, due to the fact that the cross sections for pair production and Compton scattering increase, respectively, with Z^2 and Z, and there are no excited nuclei to evaporate nucleons.

B. Description of Line-source Target

The hydrogen target (Fig. 12) used in the energy distribution measurements was designed by Cook.[10] Fig. 13 presents a cross-sectional diagram of the target and of the shielding which was built to channel the mesons and to house the crystal counters. The target constitutes a "line source" of mesons, and channelling of the mesons is thus essential. (The shielding is designed to accommodate the measurement of energy distributions of mesons at 45°, 90°, and 135°; however, complete data were taken only at 90°.)

The liquid hydrogen under bombardment is enclosed in a horizontal steel tube 2 inches in diameter, with walls 0.035 inch thick. To this

tube is connected a reservoir of liquid hydrogen sufficient to keep the target chamber filled for about four successive days without refilling. Insulation of the reservoir is accomplished by three concentric chambers, the inner and outer chambers being evacuated, the middle one filled with liquid nitrogen. In order to avoid excessive absorption of the mesons, the nitrogen chamber does not surround the target; instead, three copper foils, 5 mils in thickness, provide heat shielding around the target and are attached to the liquid nitrogen jacket.

In view of the possibility of explosion, great care was taken to exclude all air from the reservoir before filling it with hydrogen; careful consideration was also given to the method of venting the hydrogen gas evolved during the experiment.

C. Energy Distribution of Photons in the X-ray Beam

If the electrons in the synchrotron were to all strike an infinitely thin target with the same energy, the energy distribution of the photons produced would theoretically have the characteristic bremsstrahlung spectrum[13] shown in Curve A of Fig. 14. Modification of this spectrum must be made, however, for the following reasons:

a) The electron target is not infinitely thin, but consists of 20 mils of platinum.

b) Only that part of the photon beam is used which is contained in a cone having a half angle of about $1/2^{\circ}$; collimation removes the remainder of the beam.

The correction to the bremsstrahlung distribution necessitated by a) and b) was computed by Steinberger and Christian[14] and is plotted in Curve B of Fig. 14.

c) Because of the spread-out character of the electron beam (see Section III,B), the electrons do not all have the same energy upon striking the target. The energy distribution of the electron beam was determined experimentally,* however, and the corresponding correction to the photon distribution (Curve C of Fig. 14) was calculated by numerical integration.

Thus far we have found the energy distribution of photons in the x-ray beam. However, the fact that there is an angular spread in the mesons which can reach the crystal necessitates a further computation. What is needed is the number of photons which can produce mesons of a given energy. This necessitates a geometrical analysis of the target and crystal layout, in order to provide an intensity-versus-angle plot. Since at each angle there is a different relationship between meson energy and photon energy, another numerical integration is necessary in order to determine the number of photons per unit meson energy. As would be expected, the corrected distribution (see Curve B of Fig. 15) shows a knee at the high energy end.

D. Energy Distribution of Mesons

The experimental results of the energy distribution measurements from hydrogen are shown in Curve A of Fig. 15, as a function of meson energy. As before, the different meson energies were obtained by placing varying amounts of absorber between the target and the crystals. The computations leading to the determination of the cross sections are given in Appendix E.

E. Excitation Function for Meson Production

As has already been pointed out, the principal value of a measurement of the energy distribution from hydrogen is that the excitation

---

* See Appendix D.

function for meson production (i.e., cross section as a function of photon energy) may be derived therefrom. Since the number of mesons produced has been measured as a function of energy and the number of photons of a given energy in the x-ray beam may be calculated, the ratio provides a measure of the excitation function. This function is presented in Fig. 16, and again the computations are outlined in Appendix E.

VI ANGULAR DISTRIBUTION FROM LIQUID HYDROGEN

A. Description of Point-source Target

By the time the measurement of the excitation function was completed, a new hydrogen target (Fig. 17), developed by V. Peterson,[3] was available for meson research. Whereas the earlier target constituted a "line source," the new target is effectively a "point source," since the hydrogen under bombardment is contained in a small cylindrical cup of duraluminum, 1 1/2 inches in diameter, 2 inches in height, and with walls 0.002 inch thick. The advantage of such a target for measurement of angular distribution is that, with the point source, identically the same target volume is seen by the crystals at each angle.

The geometry used in the measurement of angular distribution is shown in Fig. 18. The crystals and accompanying electronics for meson detection were mounted in an aluminum box which pivoted, via a track, about the target as a center, such that measurements could be made at any desired angle. Since no collimation was needed for the mesons, it was possible to use so-called "bad" geometry: the absorbers were several times the area of the crystals, with the result that errors due to Coulomb scattering could be neglected.

Geometrical limitations made it impossible at the 45° position to place the crystals any closer than about 11 inches from the target, and still have room for the necessary amount of absorber. This fact, in conjunction with the smallness of the point-source cup, resulted in a rather low meson counting rate. For this reason, the angular distribution was measured at 30° intervals for only a single photon energy, again that of 250 Mev.

B. Angular Distribution

The results of the angular distribution are shown in Fig. 19, together with the data from the subtraction method,* plotted in terms of the angle of emission in the center of mass system. The data from the two methods are in excellent agreement. As seen, the distribution is roughly isotropic, but with a maximum in the backward direction. The theoretical interpretation of this distribution is discussed in Section VIII

* The absolute values from the subtraction method have been revised from those given in Fig. 11, as a result of the recent determination of the counting efficiency of the crystals (see Section II, G).

VII OUTLINE OF MESON THEORIES

In analogy with the highly successful quantum theory of electrodynamics, in which interaction between charged particles is accomplished through the medium of photon exchange, nuclear field theory is based on the assumption that interchange of π-mesons between nucleons is responsible for nuclear forces. The short range of these forces results immediately from non-zero mass of the π-meson.

The weight of experimental evidence accumulated to date indicates that, like the photon, the π-meson is a Bose particle (with integral spin). Under this assumption four types of meson fields are generally considered acceptable: scalar, pseudoscalar, vector, and pseudovector. The method by which these meson fields are coupled to the nuclear fields is also open to choice.

It is possible to make computations, on the basis of these theories, of the results to be expected for various processes in which nuclear forces are involved. It will be attempted here to sketch extremely briefly the predictions of each of these theories, particularly as applied to photomeson production.

Two principal methods have been used in an attempt to solve the field equations: a) the ordinary perturbation method (weak coupling method) assumes that the kinetic energies of the emitted particles are large, and treats the coupling energy as a perturbation. Thus, as in electrodynamics, the coupling constant $g^2/\hbar c$ is assumed to be small,* and the perturbation is expanded in terms of increasing powers of this coupling constant. This method may be applied straightforwardly for the

---

* In electrodynamics, the coupling constant $e^2/\hbar c = 1/137$.

case of the scalar meson, but in the case of the pseudoscalar, pseudovector, and vector meson, the terms of second and higher order are no longer small, but instead are large or infinite. Recently, the subtraction method of Schwinger and Tomonaga, so successfully applied in electrodynamics have been applied to the pseudoscalar theory (with pseudoscalar coupling) to give exact results. Weak coupling theory has not, however, been successful in dealing with mesons having unit spin.

b) An alternative procedure in performing the computations is that of introducing the concept of strong coupling: the coupling is assumed to be large, and the kinetic energy of the emitted particles is treated as a perturbation. Here the perturbation expansion is made in terms of decreasing powers of the coupling constant. Such a scheme, however, suffers from the severe difficulty of not being relativistically invariant, since the nucleon can no longer be described as a point source. The self-energy of the meson field, written in terms of an extended nuclear source of dimensions a, becomes infinite as $a \longrightarrow 0$. To date, no method of overcoming this difficulty of relativistic invariance has been developed.

These two widely differing procedures constitute the principal methods of attack in meson theory. It is now clear that the actual value of the coupling constant lies somewhere between the extremes assumed in these two methods. Hence the predicted results are surely not to be taken too seriously, but used rather as a guide to aid in the selection of the correct type of meson field and meson interaction.

A. Scalar Theory

The pure scalar theory, by definition, infers a meson without a magnetic moment (i.e., spin 0). If one were to assume that only one kind

of meson field is allowed, one could immediately reject the pure scalar theory, since scalar mesons are not coupled to the spin of the nucleon, and hence cannot explain the spin dependence of nuclear forces. Nor could one begin to explain, on the basis of such a theory, the anomolous magnetic moment of the proton and neutron.

In this theory, the meson is symmetrically distributed about the nucleon and is loosely coupled to it, much as the electron is coupled to an atom. Hence, an electromagnetic wave interacts more strongly with the meson than with the nucleon, with the result that the angular distribution of the emitted mesons is analagous to that observed in the photoeffect. The computed angular distribution[18] for 250 Mev photons is approximately the $\frac{\sin^2 \theta}{(1 - \frac{v}{c} \cos \theta)^2}$ distribution of a simple electric dipole photoeffect. It is shown in Fig. 20.

The excitation function at 90° to be expected[18] on the basis of the scalar theory increases rather slowly from threshold and flattens off, as shown in Fig. 21.

B. Pseudoscalar Theory

In order to explain, among other things, the energy difference between the triplet and singlet state of the deuteron, nuclear forces must clearly be at least partially spin dependent. This spin dependence may be introduced into the theory either through the introduction of a meson with spin different from zero, or, alternatively and less obviously, one may mathematically describe the wave function of a zero-spin meson as an antisymmetric tensor instead of a scalar. This description, which satisfies the same wave equation as the scalar meson and differs from it only in its inversion property $\phi(r) = -\phi(-r)$, is called the pseudoscalar

meson theory.

The meson field ϕ may now be coupled to the spin of the nucleus in one of two different ways:

a) Pseudovector coupling: since ϕ is a pseudoscalar in this theory, $\nabla\phi$ is a pseudovector. Since the spin $\bar{s}$ of the nucleon is a pseudovector (see below), the interaction energy is given by the scalar quantity $\bar{s} \cdot \nabla\phi$.

b) Pseudoscalar coupling: here the interaction energy is assumed to be of the form $(\phi^+ \gamma_5 \phi)\phi$, again a scalar, as required.

While the form of the coupling of the meson to the nucleon is uncertain, it may be shown that the results, for a pseudoscalar meson field, are not affected to order g^2.

In this theory of the pseudoscalar meson, the meson may be shown to be closely bound to the nucleon. As a result, the interaction between a photon and the current produced by the motion of the meson would be small, and the photon is thus predominantly coupled to the magnetic moment of the nucleon. This interaction may result in a flipping of the spin of the nucleon, with the accompanying radiation of a meson. Such an interaction, involving absorption of the photon by a nearly stationary nucleus, will provide a rather isotropic angular distribution of radiated mesons. This distribution[18] is plotted in Fig. 20, for photons of 250 Mev.

The excitation function at 90^0 to be expected[18] from the pseudoscalar theory is shown in Fig. 21. It rises more abruptly from threshold than does the scalar theory, and again flattens off at roughly the same photon energy. However, these theories which involve a close coupling between meson and nucleon lead to incorrect predictions of scattering phenomena. They predict, in fact, nuclear radii of the dimensions of the Compton wave-length

of the nucleons and are therefore hardly to be taken seriously.

C. Vector Theory

The vector meson theory, in which the meson is assumed to have unit spin, is merely the generalization of the theory of quantum electrodynamics, in which the field particle possesses a finite, rather than a zero, mass. As in electromagnetic theory, field is described in terms of a four-vector potential A.

Comparatively little attention has been paid to vector theory alone, since it predicts the wrong sign for the quadrupole moment of the deuteron. Theories involving mixtures of vector and pseudoscalar fields have, however, received a fair amount of attention. Under the assumption that the mass of the vector meson is slightly greater than that of the pseudoscalar meson, it is possible to concoct a mixture which will provide the correct sign of the quadrupole moment. The computed value, however, is several times too small.

In addition, other results are in complete disagreement with experiment. The excitation function for photomeson production, for example, increases continually with increase of photon energy and exhibits no turning point. Moreover, the angular distribution turns out to be strongly peaked in the forward direction.

D. Pseudovector Theory

By the term "pseudovector" is meant a vector which does not change sign upon inversion in the origin. Any axial vector (formed by the cross-product of two ordinary vectors) constitutes a pseudovector and hence spin $\bar{s}$ is a pseudovector. If, as is assumed in this theory, the interaction is presented in the form $\bar{s} \cdot \phi$, the field ϕ must be a

pseudovector if the interaction energy is to be a scalar.

The pseudovector theory has excited comparatively little enthusiasm, probably because, under weak coupling approximations, it gives rise to repulsive forces in both the singlet and triplet state of the deuteron, and is therefore totally unacceptable in this approximation.

The angular distribution which results from photoproduction of mesons according to this theory is reasonably isotropic and somewhat similar to that of the pseudoscalar theory. The excitation function, however, increases continuously and very rapidly from threshold and is clearly wrong.

VIII INTERPRETATION OF RESULTS; CONCLUSIONS

The results of the angular distribution (Fig. 19) show a rather flat distribution, with a slight peak in the backward direction. Such a distribution is quite incompatible with that predicted by the scalar theory (Fig. 20). In fact, the only theories which predict such a flat distribution are those in which the electromagnetic interaction is chiefly with the magnetic moment of the nucleons, rather than with the electric charge of the meson. This is so for the pseudoscalar meson theory with both types of coupling.[15] However, these theories which involve tight coupling of the mesons to the magnetic moment of the nucleon can hardly be taken seriously, in view of their incorrect predictions of nucleon-nucleon scattering, as mentioned in Section VII.

The energy distribution at 90° (Fig. 15) does not disagree violently with the predicted results of either the scalar or pseudoscalar theory, (Fig. 21) but is incompatible with the predictions of the vector and pseudovector theories, which show a rapid rise in cross section as a function of photon energy, and do not exhibit any sign of a turning point. These theories cannot, however, be completely rejected, since there remains the possibility that the theoretical computations are incorrect due to the fact that relativity and the largeness of the coupling constant are not simultaneously taken into account.

Comparison of the results of this experiment with theory is thus seen to indicate that π^{+}-mesons have zero spin and are tightly coupled to the nucleons. As discussed, the theoretical computations are not to be trusted in view of the fact that the magnitude of the coupling of mesons to nucleons lies somewhere between the extremes assumed in the

approximations of strong and weak coupling. In fact, it may be seen that the experimental data are best fitted,[16] for pseudoscalar mesons with pseudoscalar coupling, if the coupling constant $g^2/4\pi\hbar c$ is chosen to be about 20.

IX APPENDIX

A. Calculation of Relationship between (k, T_π, θ)

Using the notation

M_p = rest mass of struck particle (a proton, in this case)

M_n = rest mass of struck particle after collision (a neutron, in this case)

M_π = rest mass of the meson

k = energy in laboratory system of the incident particle (here a photon)

E_n = total energy in laboratory system of the neutron

T_π = kinetic energy of the meson

$\Delta M = M_p - M_n$

θ = angle in laboratory system between the emitted meson and the direction of the incident photon

etc.,

we have the following relationships:

a) energy conservation: $k + M_p c^2 = E_n + E_\pi$

b) momentum conservation: $\overline{P}_k = \overline{P}_\pi + \overline{P}_n$,

$$\text{where } P_\pi c = \sqrt{T_\pi^2 + 2T_\pi M_\pi c^2}$$

etc.

solving for k in terms of θ and T_π, we have

$$k = \frac{(2M_p c^2 + \Delta M c^2)\Delta M c^2 - M_n^2 c^4 + 2M_\pi c^2 M_p c^2 + 2T_\pi M_p c^2}{2\left\{M_p c^2 - M_\pi c^2 - T_\pi + \cos\theta \left[T_\pi^2 + 2T_\pi M_\pi c^2\right]^{1/2}\right\}}$$

Equation (1) of page 7 is derived immediately from this relationship.

B. Typical Data Sheet
(Angular Distribution of Mesons by Carbon-Polyethylene Subtraction)

Run No.	Beam Integrator	Time in Minutes	Absorber Thickness	Target	Angle	I	II_a	II_b	G	Delayed Coincidence				Calculated Background
										1	2	3	4	
98-1	20.0	16.5	$\frac{3}{4}$" Alum.	Carbon	135°	37.3x256	21.0x256	147.8x256	13.3x256	133	50	41	27	18.2
98-2	20.0	14.1	"	Poly	"	34.0x256	19.7x256	139.7x256	10.5x256	178	72	34	25	18.7
98-3	20.0	14.2	$1\frac{1}{4}$" Alum.	Carbon	$112\frac{1}{2}$°	34.5x256	21.2x256	98.4x256	11.2x256	92	44	20	19	14.0
98-4	20.0	15.8	"	Poly	"	32.4x256	19.8x256	89.5x256	11.8x256	167	63	27	16	12.0
98-5	20.0	18.5	2" Alum.	Carbon	90°	35.0x256	21.6x256	119.1x256	10.7x256	94	33	13	17	12.5
98-6	20.0	19.5	"	Poly	"	33.2x256	21.0x256	106.1x256	11.1x256	138	53	19	17	10.8

Notation:

I = number of large pulses (energy loss >6 Mev) in crystal No. I

II_a = number of large pulses (energy loss >5 Mev) in crystal No. II

II_b = number of smaller pulses (energy loss $>$ about 2 Mev) in crystal No. II

G = number of coincidences between pulses I and II_a

Delayed coincidences No. 1 = coincidences between the first delayed gate and II_b. These coincidences include both mesons and random background (computed in the last column).

C. Outline of the Electronics

1. Phototube Circuit and Cathode Follower

In all of this research, 1P21 phototubes were used, connected in the conventional way shown in Fig. 22. A negative voltage of 600-1000 volts was applied to the first collector plate. The purpose of the cathode follower was merely to ensure transmission of the signal through the 60 odd feet of coaxial cable running from the bombardment room to the electronics room. (It was found possible, actually, to dispense with the cathode follower and to connect the output of the phototube directly into the coaxial line, if desired.)

2. Linear Amplification

A linear amplification stage (Fig. 22), with a gain of about 100, and a band width of 10 mc, was used between the photomultiplier circuit and the pulse shaping circuit.

3. Pulse Shaper and Discriminator

A very effective pulse shaper and discriminator, developed principally by Mr. Louis Wouters, was used in this research and is shown in Fig. 23. This circuit accepts negative pulses of 0.1 - 0.2 volts, amplifies them with a wide band-pass amplifier, performs the discrimination between the third and fourth stages at a level of about 30 volts, and provides positive feedback from the fourth stage to the second stage to square up the pulses. The potentiometers at the input and output of the linear amplifier stage served to set the level of discrimination.

4. Coincidence-anticoincidence Circuit

The coincidence-anticoincidence circuit used in this work is shown in Fig. 24. This circuit, together with a simplified version which omits the anticoincidence function, has a coincidence ratio (defined as

$\left(\frac{\text{output voltage with coincidence}}{\text{output voltage without coincidence}}\right)$ of about 7 : 1.

5. Gate Circuit

The electronics for constructing the four successively-delayed gates is shown in Fig. 25. Since there was no need for adjustment of the gate lengths, they were determined by delay lines built into the circuit.

D. Correction to the Energy Distribution of Photons

The intensity of the electron beam as a function of time (as seen with a beam monitor oscilloscope) is given in Fig. 3. By comparison with the theoretical variation of the beam energy versus time (also given in Fig. 3), a plot of beam intensity versus beam energy was made. Utilizing Curve B of Fig. 14, a numerical integration was then made over the variation in intensity and energy. The corrected curve is given in Curve C of Fig. 14.

E. Calculation of Absolute Cross Section

By definition, $\sigma(E_{ph})$, the excitation function at 90° for photomeson production from protons, constitutes the probability that a photon of energy E_{ph}, interacting with a proton, will produce a meson at 90° in the laboratory system. Thus, the number of mesons produced per unit meson energy per unit steradian per Q, from a single proton in the target (i.e., $\frac{d^2N}{d\Omega dE_m} \times Q^{-1}$) = (the number of photons per unit meson energy per Q) x $\frac{d\sigma(E_{ph})}{d\Omega}$, where Q is defined below.

The absolute values of these quantities will now be determined.

1. Evaluation of the number of photons per unit meson energy per Q

If the total energy in the beam is E_T, and if the energy distribution of photons in the synchrotron beam followed a k/E distribution,

then the number of photons per unit photon energy would be simply $n(E_{ph}) = \frac{E_T}{E_{max} E} = \frac{Q}{E}$ (where Q is defined* to be E_T/E_{max}) since $E_T = \int_{E=0}^{E=E_{max}} k/E \; E \, dE = k \, E_{max}$. Thus the number of photons per unit meson energy per Q would be $n(E_m) = 1/E \; \frac{d E_{ph}}{d E_m}$.

The energy distribution of the photons does not, however, follow exactly a k/E distribution, but possesses, after the various corrections are made, the shape shown in Fig. 15. In effect, $n(E_m) = \frac{1}{E} \frac{dE_{ph}}{dE_m} F(E_m)$ where $F(E_m)$ is a correction factor. $F(E_m)$ has a value very close to unity for meson energies in the region of 60 Mev; hence, in the assignment of absolute values in Fig. 15, the correct distribution was normalized to the 1/E distribution in this energy region.

2. Evaluation of $\frac{d^2N}{d\Omega dE_m} \cdot Q^{-1}$

The experimental data provide the number (M/r) of mesons counted in the crystal, per r, where the r is the unit of exposure as measured by the large ionization chamber used to monitor the beam.

The number $\frac{d^2N}{d\Omega dE_m} \times Q^{-1}$ of mesons produced per unit energy per unit steradian per Q, from a single target proton, is thus related to the number of mesons counted, per r, by the equation:

$$M/r = \left(\frac{\text{no. of hydrogen atoms}}{cm^2} \right) \times \frac{d^2N}{d\Omega dE_m} \Delta\Omega \Delta E_m \times (Q/r)$$

where $\Delta E_m = \frac{dE_m}{dR} \Delta R$ is determined by the thickness ΔR of the crystal; for this experiment, $\Delta R = 2.5$ grams/cm^2 of carbon. The quantity Q is determined from the experimental data of Blocker, Kenney and Panofsky[17]

---

* Q may be regarded as the number of "photons" of energy E_{max} which are equivalent to the total energy of the beam.

and from geometrical considerations to have a value of 1.4×10^9 photons per r .

3. Evaluation of the excitation function

The excitation function $\frac{d\sigma(E_{ph})}{d\Omega}$ is evaluated merely by division of the two quantities found above.

F. Lifetime Data

No attempt was made in these experiments to determine the lifetime of the μ^+-meson with any precision. The gate lengths were never measured to better than 5 percent, and no attempt was made to provide fast rise and fall times for the gate pulses. Nor was any serious effort made to minimize the "dead time" of the shaping circuit for the II_b pulse.

In view of these facts the measured mean lifetime, as read from the four "meson" scalars (after background subtraction) serves mainly as an argument to convince oneself that the apparatus is actually counting mesons. Fig. 26 presents the lifetime data from the three sets of runs: a) energy distribution by subtraction; b) energy distribution from hydrogen; c) angular distribution from hydrogen. The three mean-life values of 2.17 μs, 2.39 μs, and 2.36 μs, (with probable errors of about $\pm$ 0.20 μs) are in satisfactory agreement with the accepted mean-life value of 2.15 μs.

X ACKNOWLEDGMENTS

I should like to express my gratitude to Dr. Jack Steinberger, for suggesting the research problem and for guiding its progress throughout its entirety. To him belongs the credit for adapting the delayed-coincidence counting technique of Rasetti to the special problem of meson detection at the synchrotron.

I am indebted to Professor E. O. Lawrence for making available this exceptional opportunity for graduate research, and to Professor E. M. McMillan for his suggestions and for his sustained interest in this problem. My sincere thanks also go to Professor R. Thornton, to Professor C. Richman, and especially to Dr. K. Brueckner, for helpful discussions of many aspects of this work. To Mr. Walter Gibbins, Mr. George McFarland, and the synchrotron crew goes the credit for furnishing a generous photon beam for these experiments. Thanks are also given to Mr. Walter Basinger for his assistance in performing the experiments. Dr. Vincent Peterson and Mr. Leslie Cook were responsible for the design of the liquid hydrogen targets. The crystals were kindly provided by Dr. Segrè and Dr. Leininger. I am grateful to Miss Betty Summers for preparing the figures used in this report.

XI REFERENCES

1. E. Gardner and C. M. G. Lattes, Science 107, 270 (1948)

2. McMillan, Peterson, and White, Science 110, 579 (1949)

3. Cartwright, Richman, Whitehead, and Wilcox, Phys. Rev. 78, 823 (1950)
   V. Z. Peterson, Phys. Rev. 79, 407 (1950)

4. O. Chamberlain, R. F. Mozley, J. Steinberger, and C. Wiegand, Phys. Rev. 79, 394 (1950)

5. N. Nereson and B. Rossi, Phys. Rev. 64, 199 (1943)
   Alvarez, Longacre, Ogren, and Thomas, Phys. Rev. 77, 752 (1950)

6. G. Gauer and C. Nunan, UCRL-714

7. F. Rasetti, Phys. Rev. 60, 198 (1941)
   J. Steinberger and A. S. Bishop, Phys. Rev. 78, 493 (1950)

8. Camerini, Fowler, Lock, and Muirhead, Phil. Mag. 41, 413 (1950)

9. J. M. Peterson, Phys. Rev., to be published

10. Leslie J. Cook, to be published

11. J. Steinberger and A. S. Bishop, Phys. Rev. 78, 494 (1950)

12. G. Chew and H. Lewis, private communication

13. See, for example, Heitler, "Quantum Theory of Radiation," 2nd Ed., p. 166 (1944), Oxford Press

14. J. Steinberger and R. Christian, private communication

15. Feshback and Lax, Phys. Rev. 76, 134 (1949)
    K. Brueckner, Phys. Rev., in press

16. K. Brueckner, private communication

17. Blocker, Kenney, and Panofsky, Phys. Rev. 79, 419 (1950)

18. These computations were performed by J. Steinberger, private communication

XII LIST OF ILLUSTRATIONS

Fig. 15 Energy distribution of π^+-mesons, produced at 90° from hydrogen and of the photons responsible for their production. The quantity Q is defined to be the energy in the x-ray beam divided by the maximum energy.

Fig. 16 Excitation function for meson production at 90° from hydrogen, with and without corrections for nuclear absorption.

Fig. 17 Photograph of the point-source target.

Fig. 18 Cross sectional view of the point-source target.

Fig. 19 Angular distribution (in center of mass system) of π^+-mesons produced in hydrogen by 250 Mev photons (laboratory system), with and without corrections for nuclear absorption.

Fig. 20 Theoretical angular distribution of scalar and pseudoscalar mesons produced by 250 Mev (laboratory system) photons on hydrogen.

Fig. 21 Theoretical cross section for the photoproduction of scalar and pseudoscalar mesons from hydrogen, as a function of photon energy.

Fig. 22 Photomultiplier circuit and linear amplifier.

Fig. 23 Pulse shaper and discriminator circuit.

Fig. 24 Coincidence-anticoincidence circuit.

Fig. 25 Four channel gate circuit.

Fig. 26 Relative number of counts in the four delayed channels, for three sets of data.

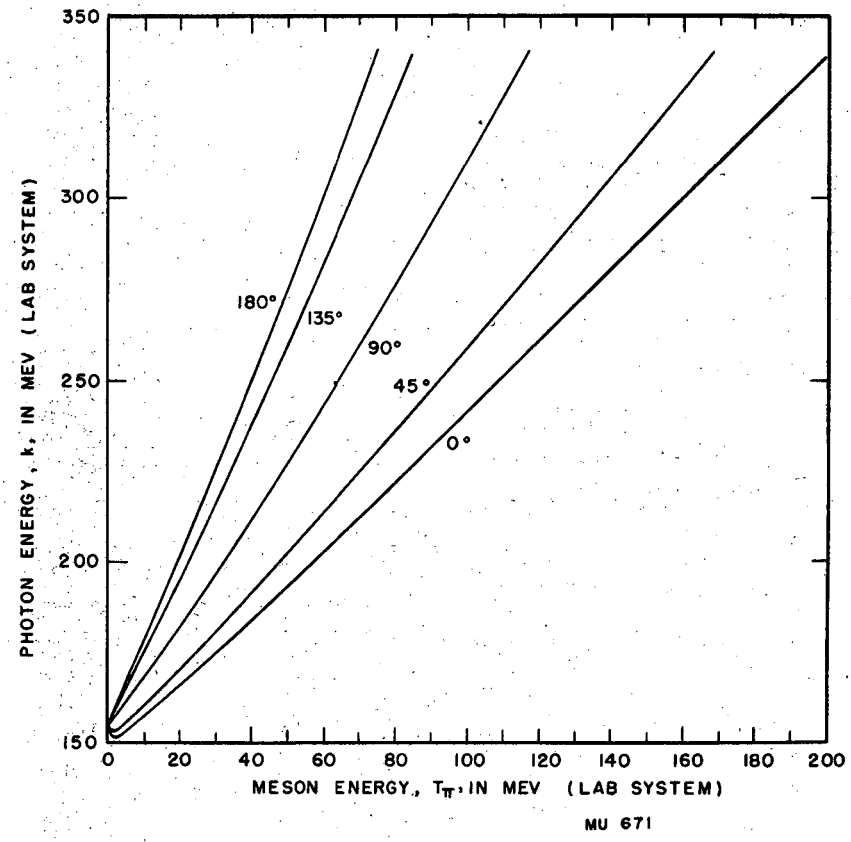
350
300
250
200
150
0
20
40
60
80
100
120
140
160
180
200
180°
135°
90°
45°
0°
PHOTON ENERGY, k, IN MEV (LAB SYSTEM)
MESON ENERGY, T_π, IN MEV (LAB SYSTEM)
MU 671

FIG. 1

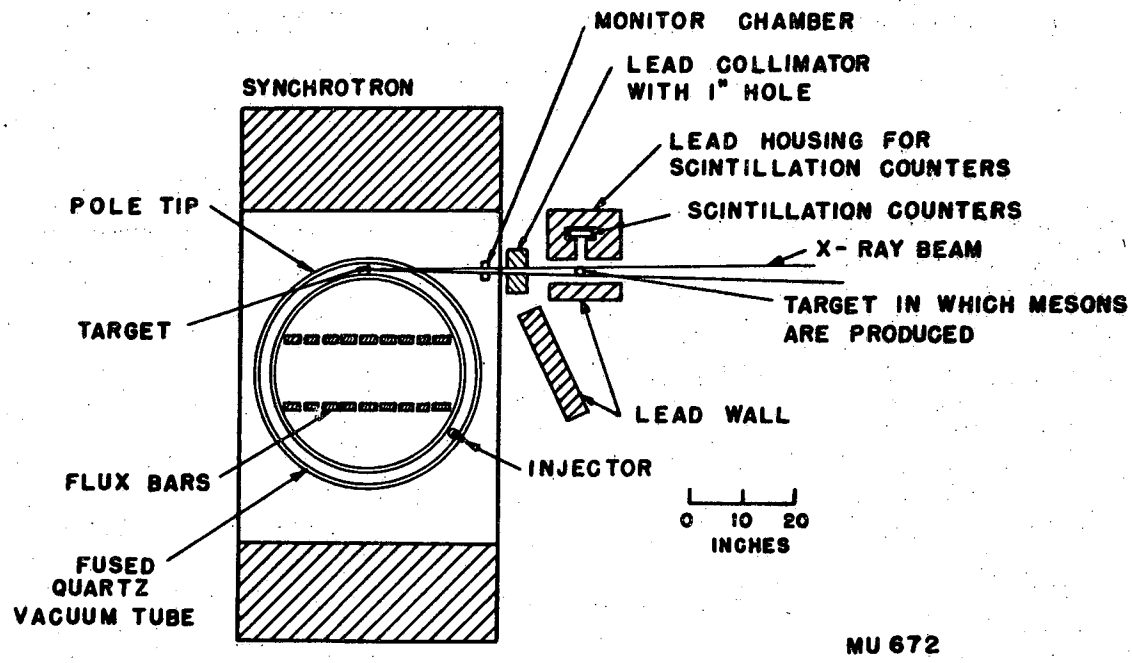
MONITOR CHAMBER
LEAD COLLIMATOR WITH 1" HOLE
SYNCHROTRON
LEAD HOUSING FOR SCINTILLATION COUNTERS
POLE TIP
SCINTILLATION COUNTERS
X- RAY BEAM
TARGET IN WHICH MESONS ARE PRODUCED
TARGET
LEAD WALL
INJECTOR
FLUX BARS
0 10 20
INCHES
FUSED QUARTZ VACUUM TUBE
MU 672

FIG. 2

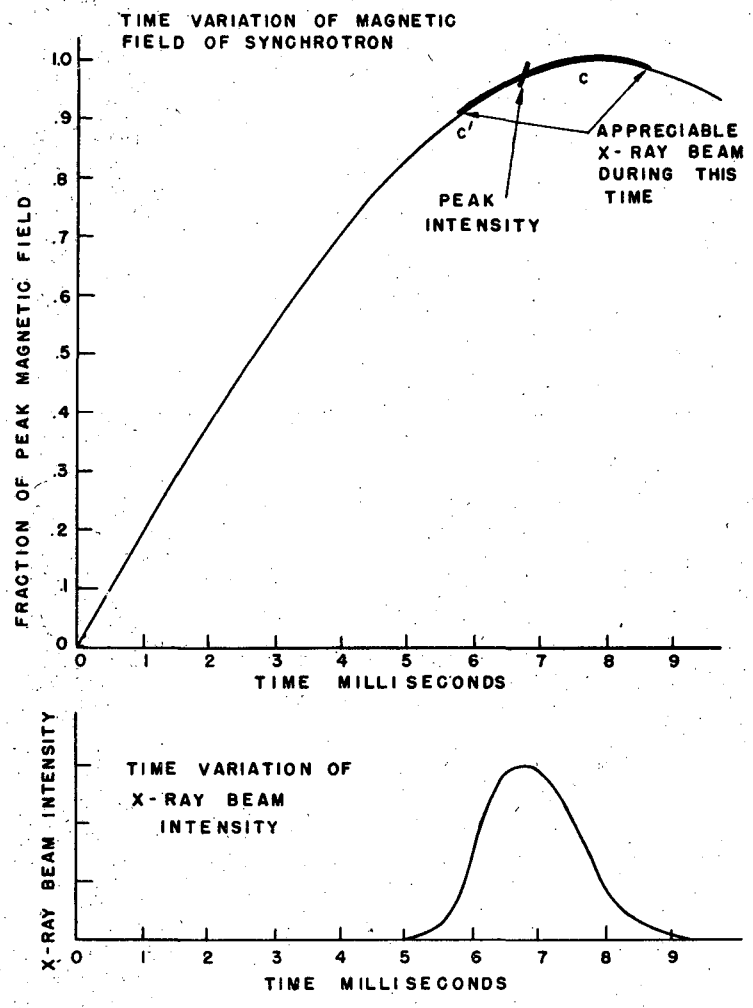
TIME VARIATION OF MAGNETIC FIELD OF SYNCHROTRON
FRACTION OF PEAK MAGNETIC FIELD
1.0
.9
.8
.7
.6
.5
.4
.3
.2
.1
0
C
C'
APPRECIABLE X-RAY BEAM DURING THIS TIME
PEAK INTENSITY
0 1 2 3 4 5 6 7 8 9
TIME MILLI SECONDS
X-RAY BEAM INTENSITY
TIME VARIATION OF X-RAY BEAM INTENSITY
0 1 2 3 4 5 6 7 8 9
TIME MILLI SECONDS
MU 247

FIG. 3

14953-I

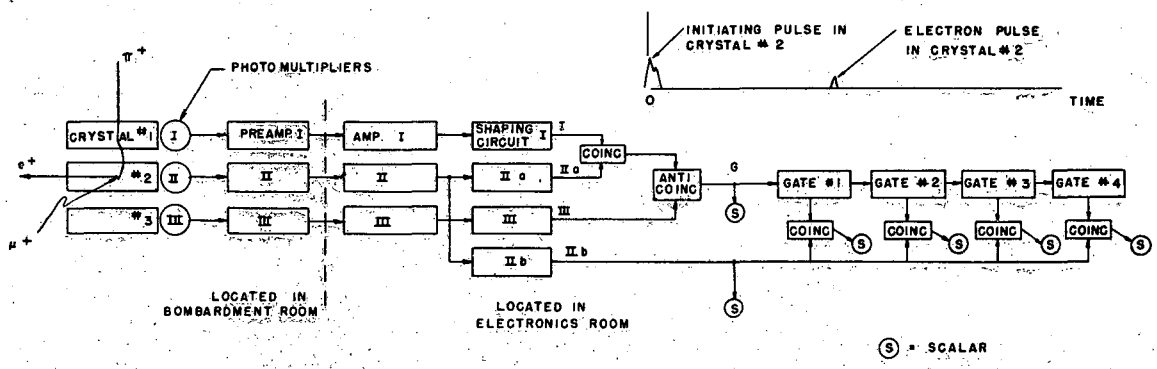
INITIATING PULSE IN CRYSTAL # 2
ELECTRON PULSE IN CRYSTAL # 2
0
TIME
π+
PHOTO MULTIPLIERS
CRYSTAL #1
#2
#3
e+
μ+
I
II
III
PREAMP. I
AMP. I
SHAPING CIRCUIT
COINC
ANTI COINC
G
GATE #1
GATE #2
GATE #3
GATE #4
IIa
IIb
LOCATED IN BOMBARDMENT ROOM
LOCATED IN ELECTRONICS ROOM
S = SCALAR
MU 673

FIG. 4

16497L

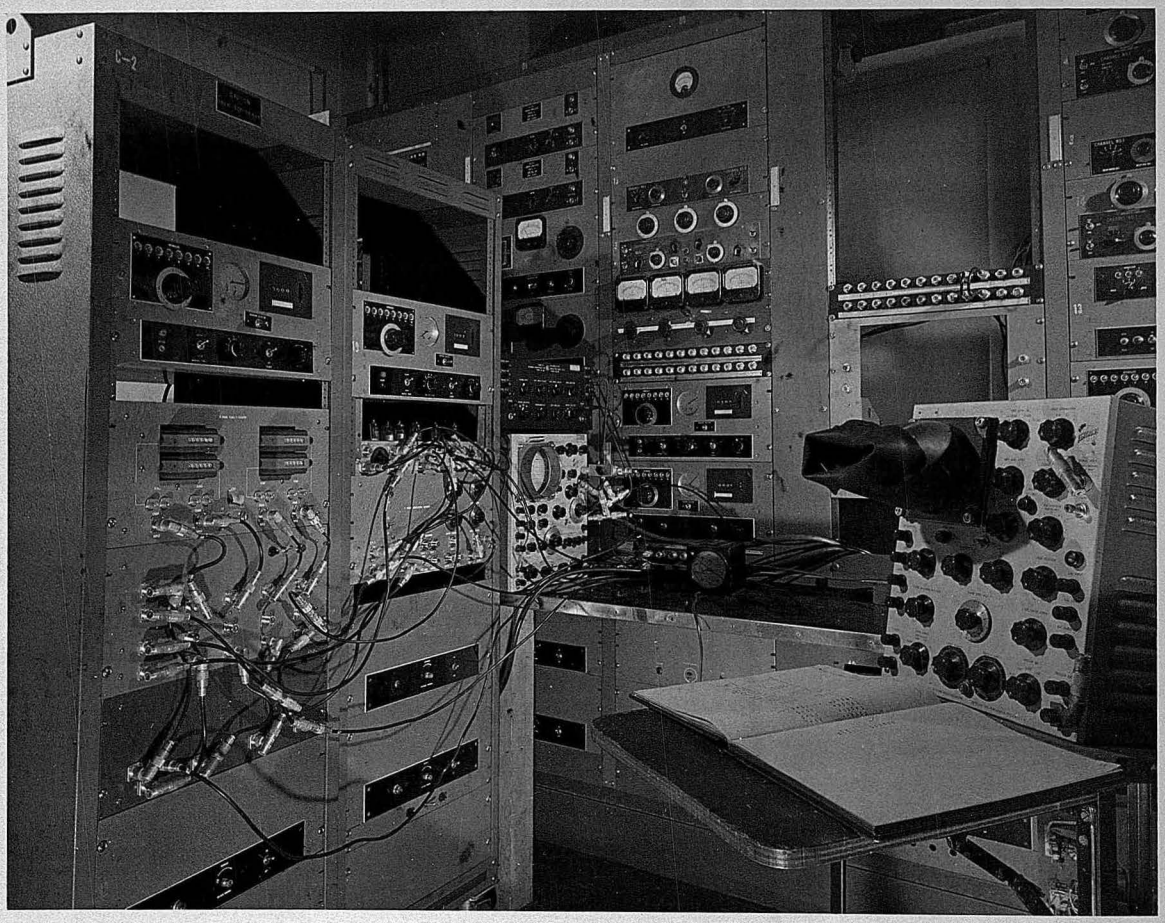

FIG. 5

ELECTRONIC EQUIPMENT

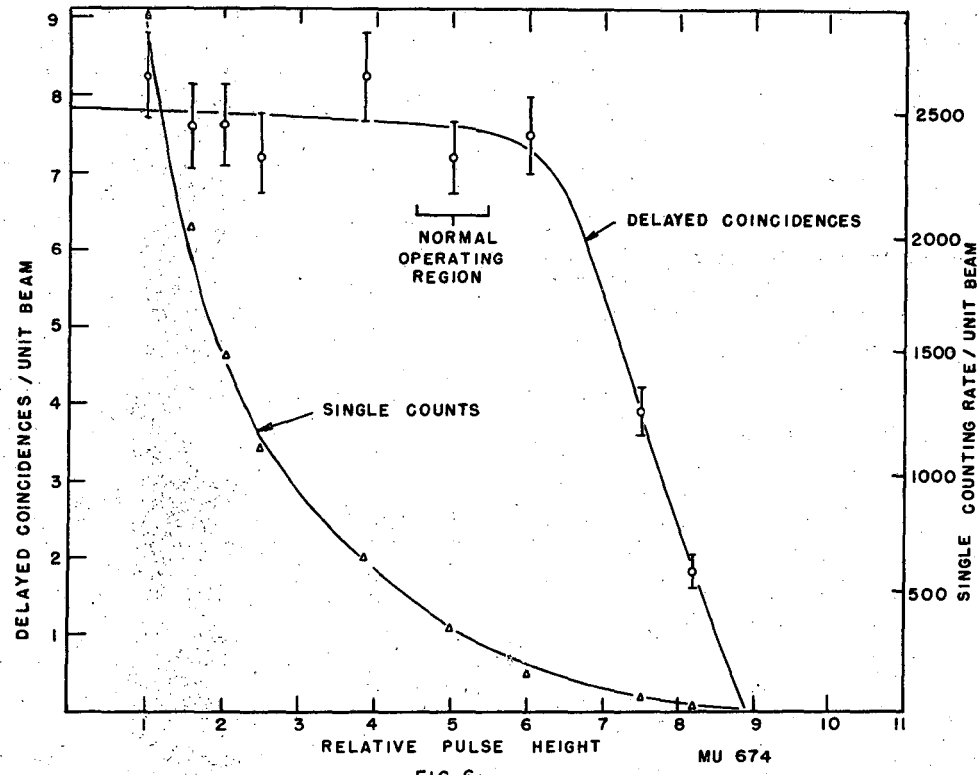
DELAYED COINCIDENCES / UNIT BEAM
SINGLE COUNTING RATE / UNIT BEAM
DELAYED COINCIDENCES
SINGLE COUNTS
NORMAL OPERATING REGION
RELATIVE PULSE HEIGHT
MU 674
1
2
3
4
5
6
7
8
9
10
11
500
1000
1500
2000
2500

FIG. 6

164981

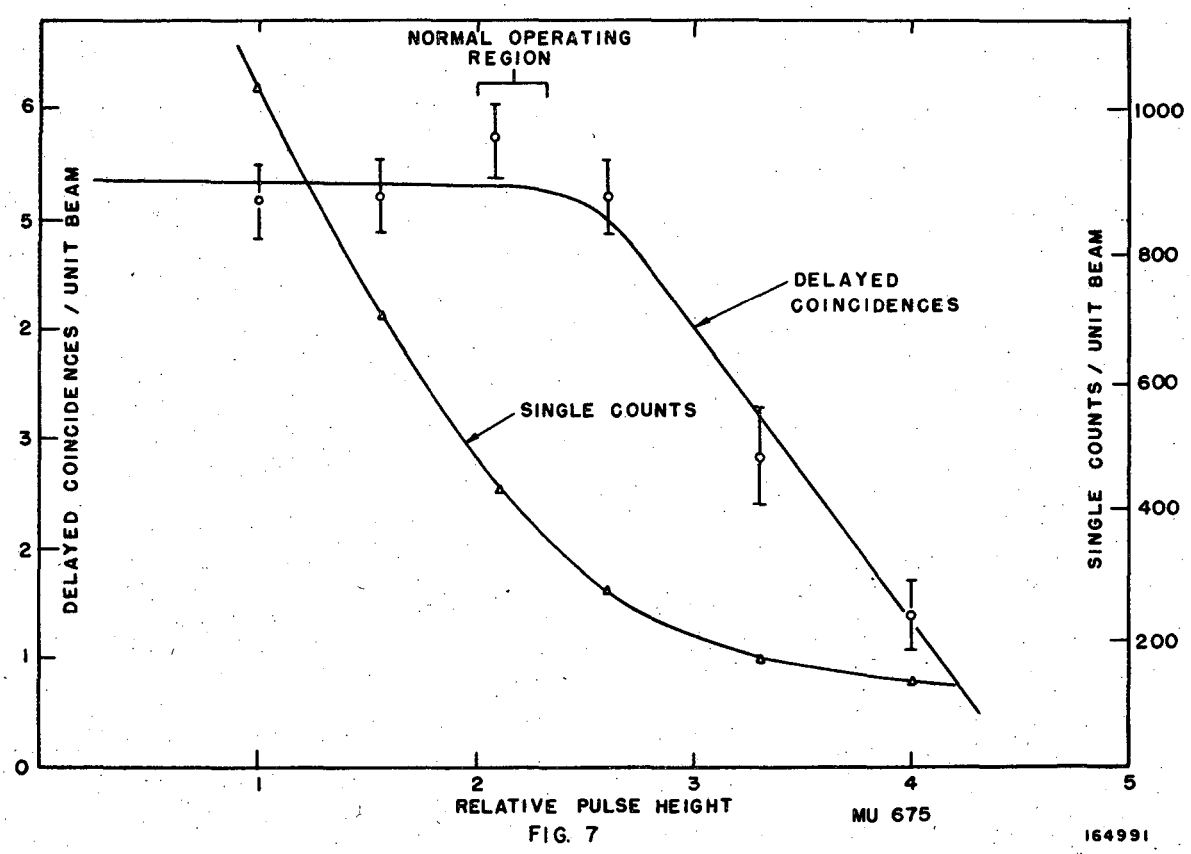

FIG. 7

MU 675

164991

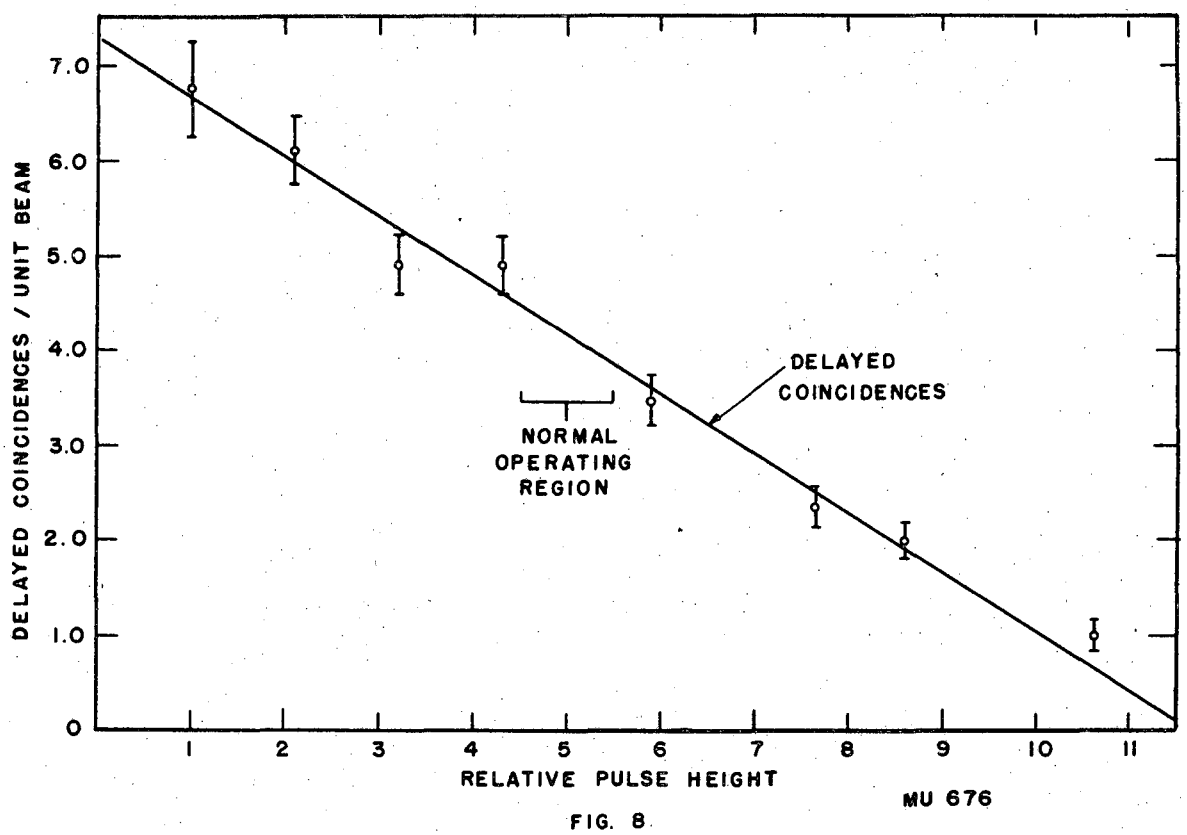
DELAYED COINCIDENCES / UNIT BEAM
7.0
6.0
5.0
4.0
3.0
2.0
1.0
0
1
2
3
4
5
6
7
8
9
10
11
RELATIVE PULSE HEIGHT
DELAYED
COINCIDENCES
NORMAL
OPERATING
REGION
MU 676

FIG. 8

165031

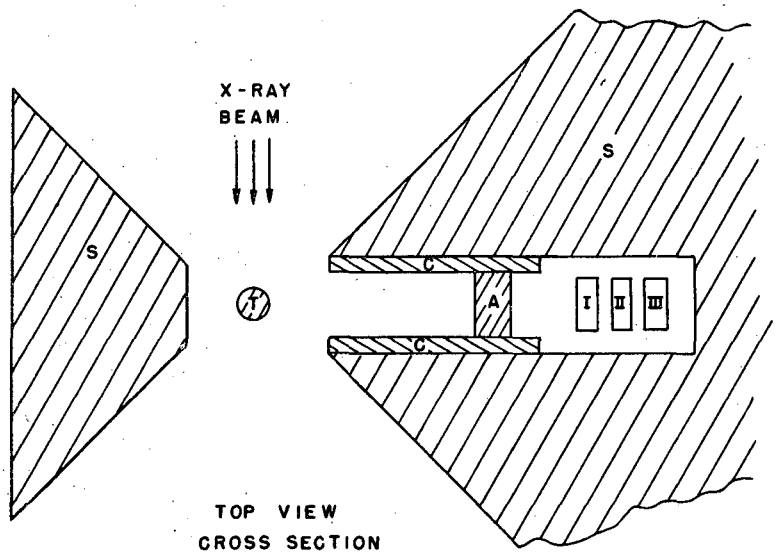

(T) TARGET
(C) Al CHANNEL
(A) Al ABSORBER
I,II,III SCINTILLATION CRYSTALS
(S) SHIELDING

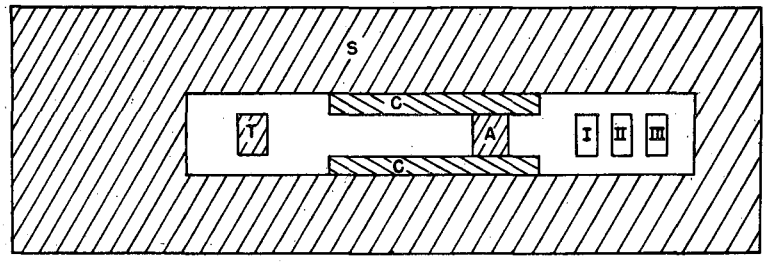

FRONT VIEW
CROSS SECTION MU 677

LOOKING INTO X-RAY BEAM

FIG. 9

165041

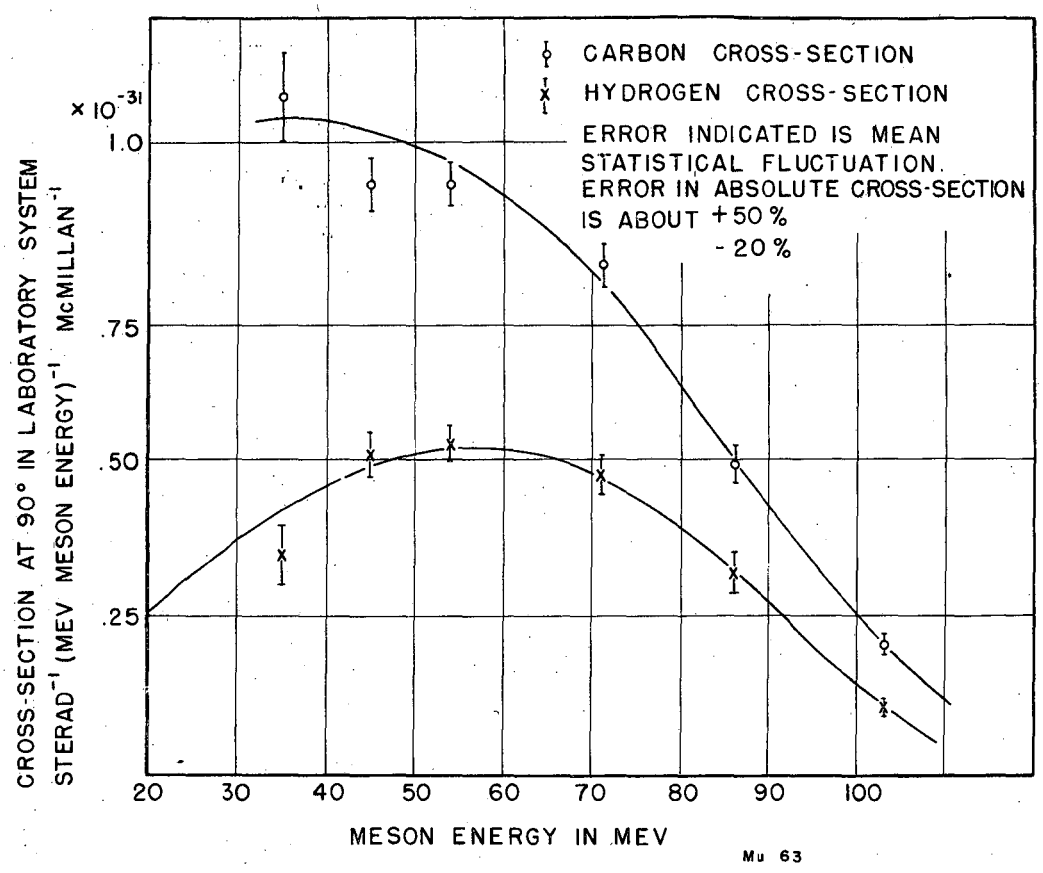
CARBON CROSS-SECTION
HYDROGEN CROSS-SECTION
ERROR INDICATED IS MEAN STATISTICAL FLUCTUATION.
ERROR IN ABSOLUTE CROSS-SECTION IS ABOUT +50 %
-20 %
× 10^-31
1.0
.75
.50
.25
CROSS-SECTION AT 90° IN LABORATORY SYSTEM
STERAD^-1 (MEV MESON ENERGY)^-1 McMILLAN^-1
20
30
40
50
60
70
80
90
100
MESON ENERGY IN MEV
Mu 63

Fig. 10

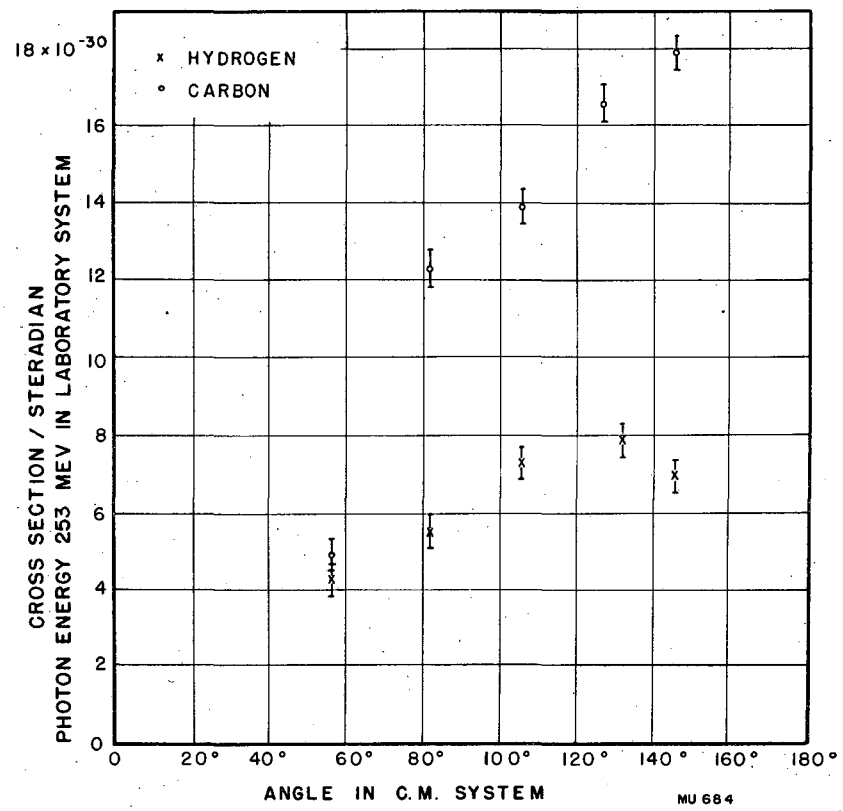
18 x 10^-30
x HYDROGEN
° CARBON
CROSS SECTION / STERADIAN
PHOTON ENERGY 253 MEV IN LABORATORY SYSTEM
0
2
4
6
8
10
12
14
16
0
20°
40°
60°
80°
100°
120°
140°
160°
180°
ANGLE IN C.M. SYSTEM
MU 684

FIG. II

FIG. 12

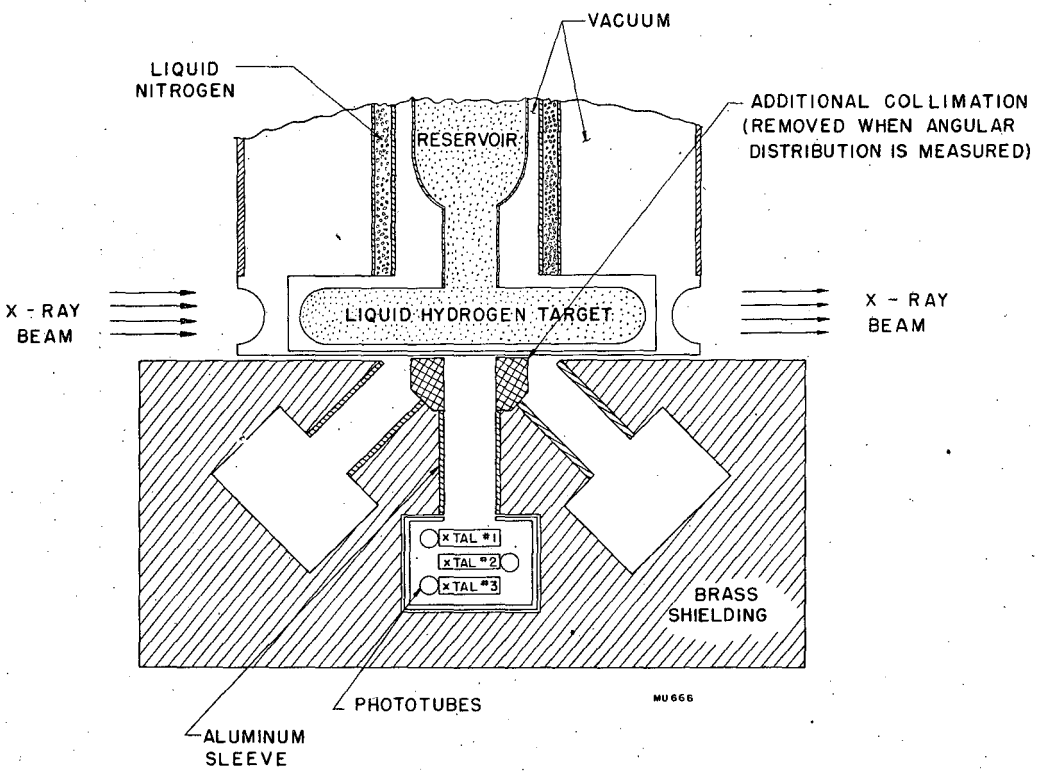

FIG. 13

14759-3

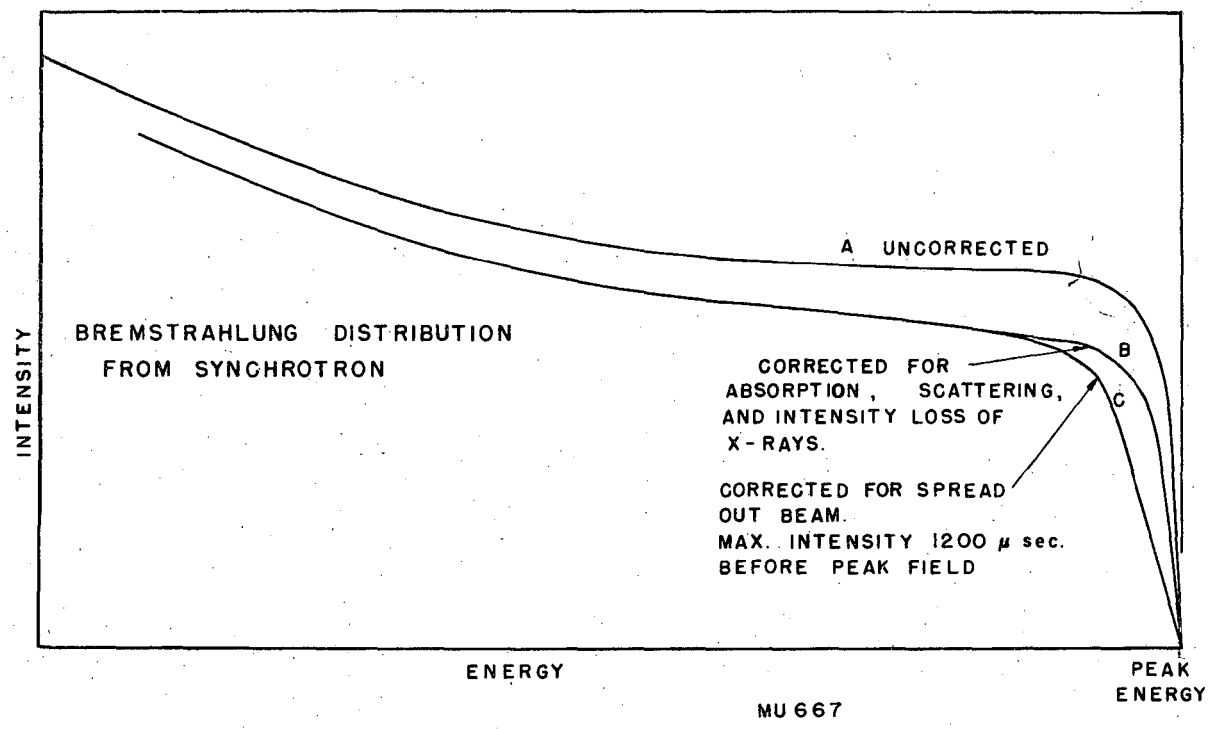
A UNCORRECTED
BREMSTRAHLUNG DISTRIBUTION
FROM SYNCHROTRON
B
CORRECTED FOR
ABSORPTION, SCATTERING,
AND INTENSITY LOSS OF
X-RAYS.
C
CORRECTED FOR SPREAD
OUT BEAM.
MAX. INTENSITY 1200 μ sec.
BEFORE PEAK FIELD
INTENSITY
ENERGY
PEAK
ENERGY

MU 667

FIG. 14

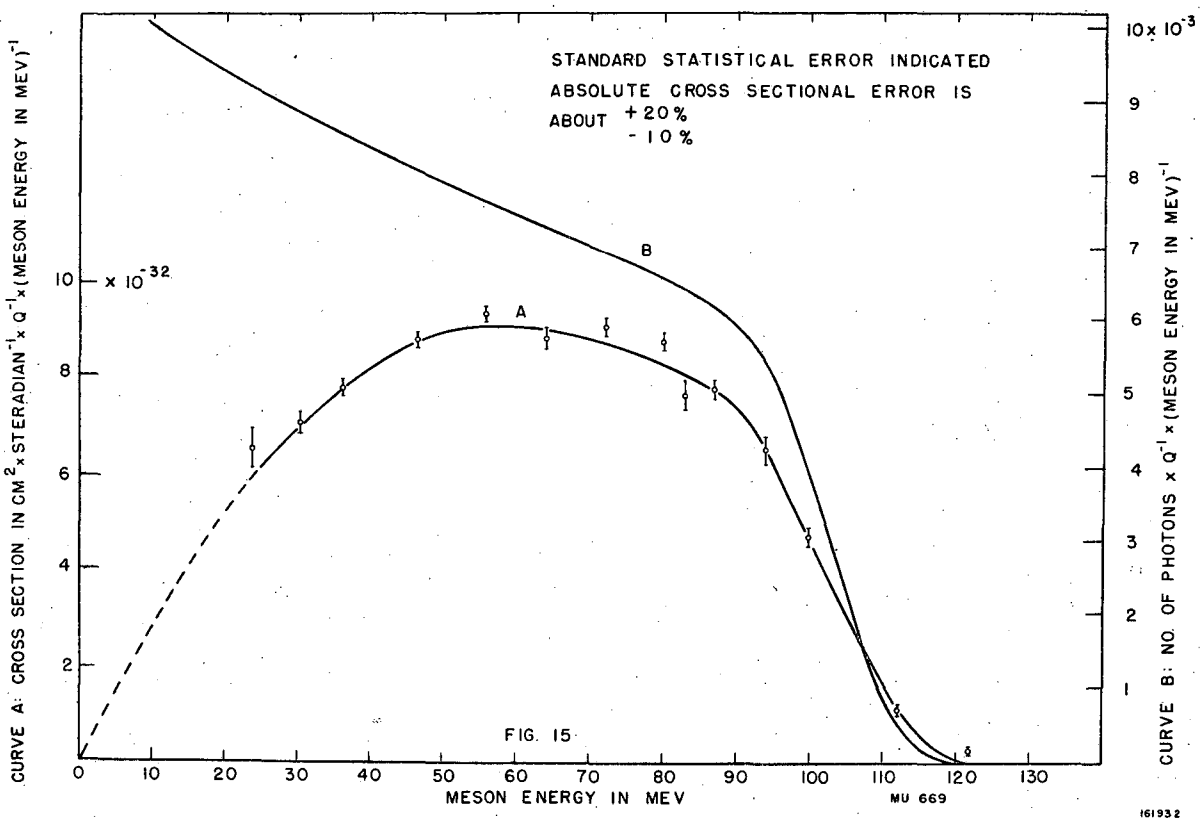
STANDARD STATISTICAL ERROR INDICATED
ABSOLUTE CROSS SECTIONAL ERROR IS
ABOUT +20%
-10%
B
A
x 10^-32
10 x 10^-3
CURVE A: CROSS SECTION IN CM^2 x STERADIAN^-1 x Q^-1 x (MESON ENERGY IN MEV)^-1
CURVE B: NO. OF PHOTONS x Q^-1 x (MESON ENERGY IN MEV)^-1
MESON ENERGY IN MEV
MU 669
161932

FIG. 15

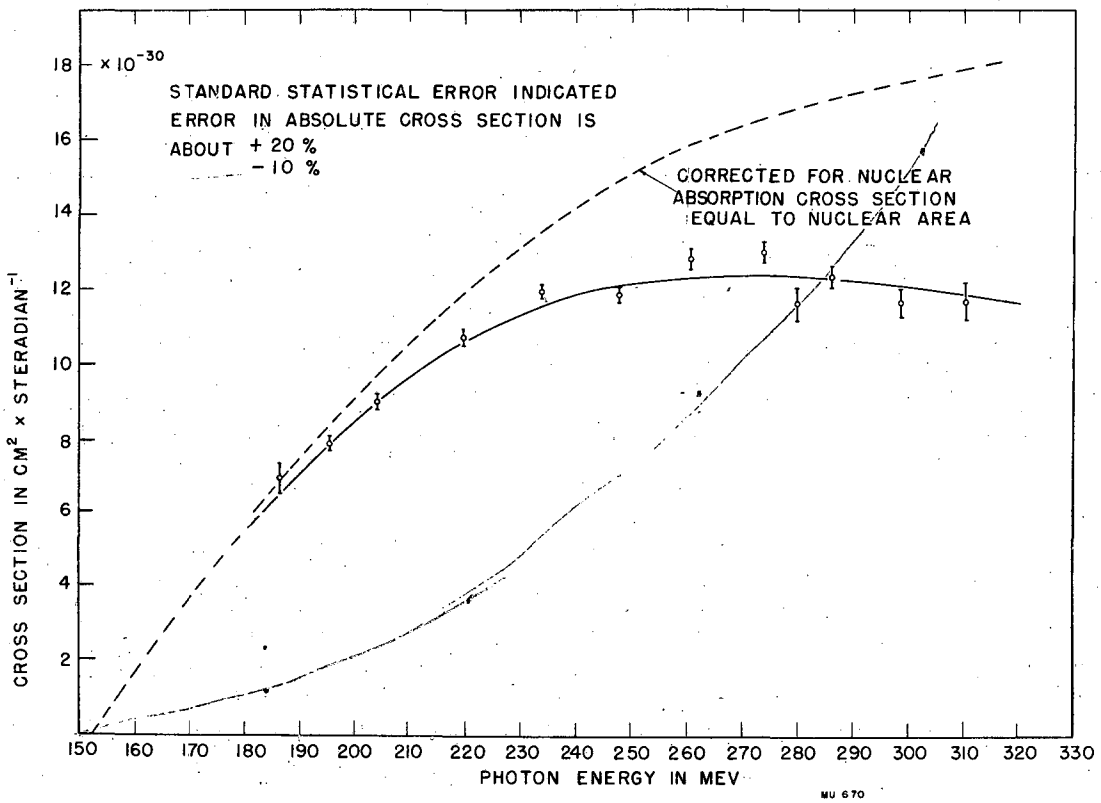
× 10⁻³⁰
STANDARD STATISTICAL ERROR INDICATED
ERROR IN ABSOLUTE CROSS SECTION IS
ABOUT + 20 %
− 10 %
CORRECTED FOR NUCLEAR
ABSORPTION CROSS SECTION
EQUAL TO NUCLEAR AREA
CROSS SECTION IN CM² × STERADIAN⁻¹
PHOTON ENERGY IN MEV
MU 670

FIG. 16

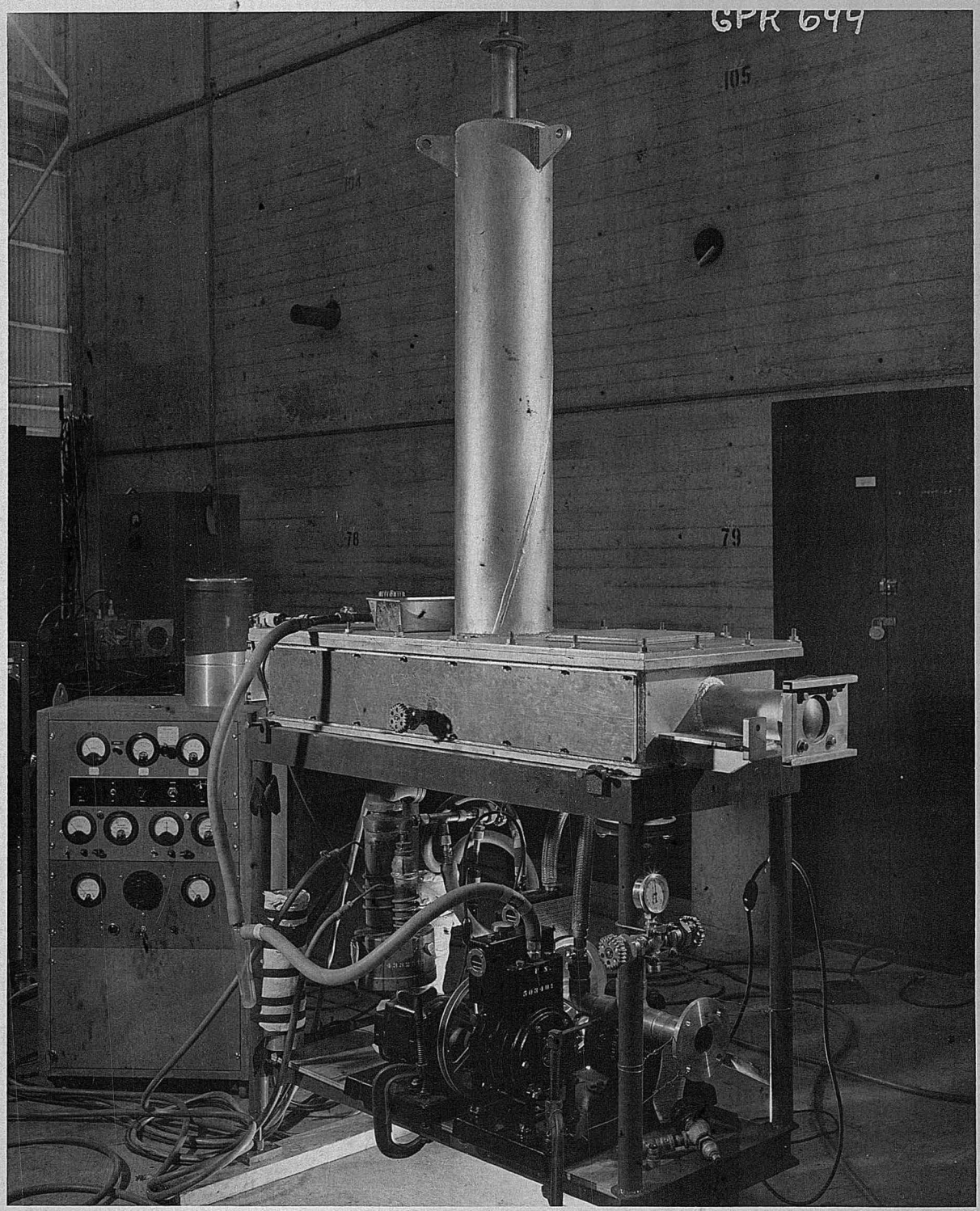

FIG. 17

LIQUID HYDROGEN TARGET WITH PUMPING SYSTEM

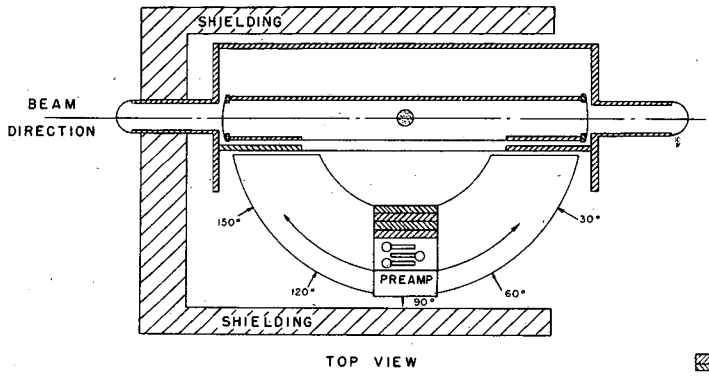

TOP VIEW

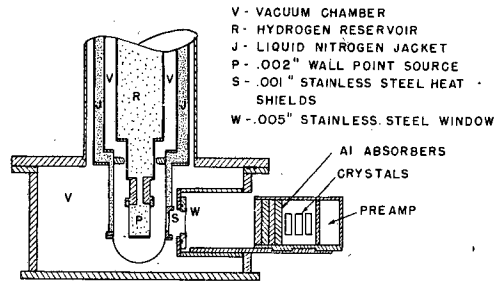

CROSS-SECTIONAL VIEW OF LIQUID HYDROGEN TARGET. (LOOKING ALONG BEAM DIRECTION)

MU 676

FIG. 18

165052

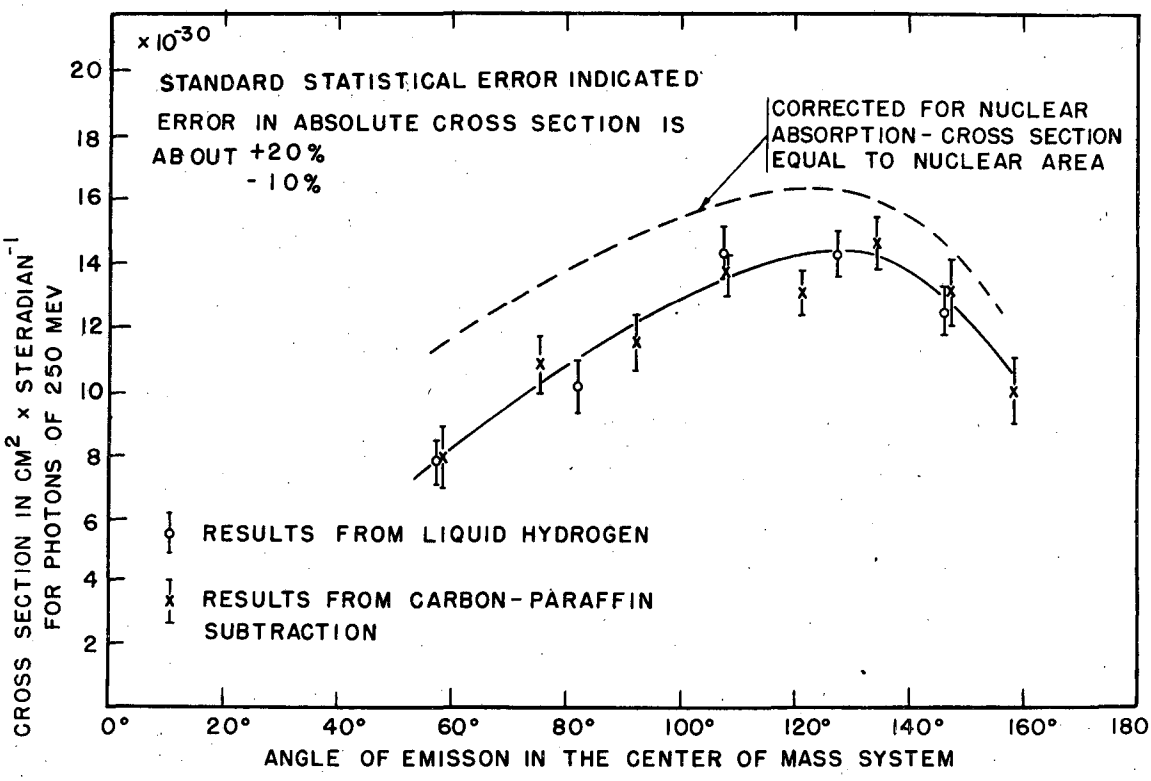

FIG. 19 MU 668

161921

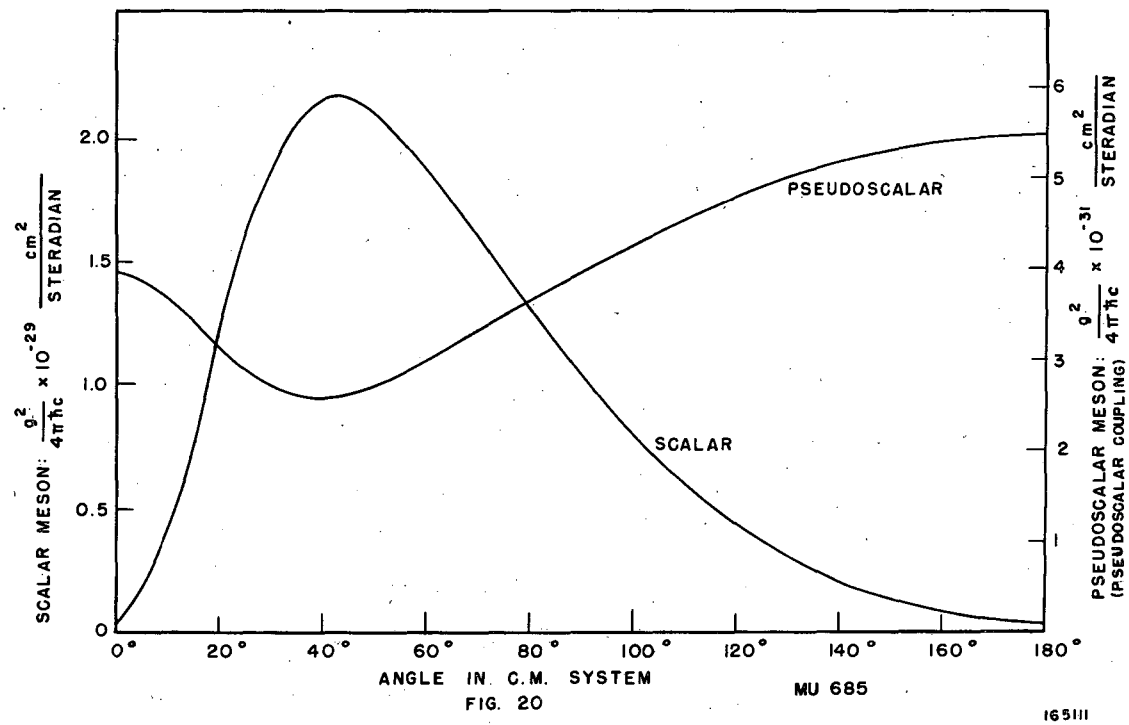
SCALAR MESON: $\frac{g^2}{4\pi\hbar c} \times 10^{-29}$ $\frac{cm^2}{STERADIAN}$
PSEUDOSCALAR MESON: $\frac{g^2}{4\pi\hbar c} \times 10^{-31}$ $\frac{cm^2}{STERADIAN}$
(PSEUDOSCALAR COUPLING)
PSEUDOSCALAR
SCALAR
0
0.5
1.0
1.5
2.0
1
2
3
4
5
6
0°
20°
40°
60°
80°
100°
120°
140°
160°
180°
ANGLE IN C.M. SYSTEM
MU 685
165111

FIG. 20

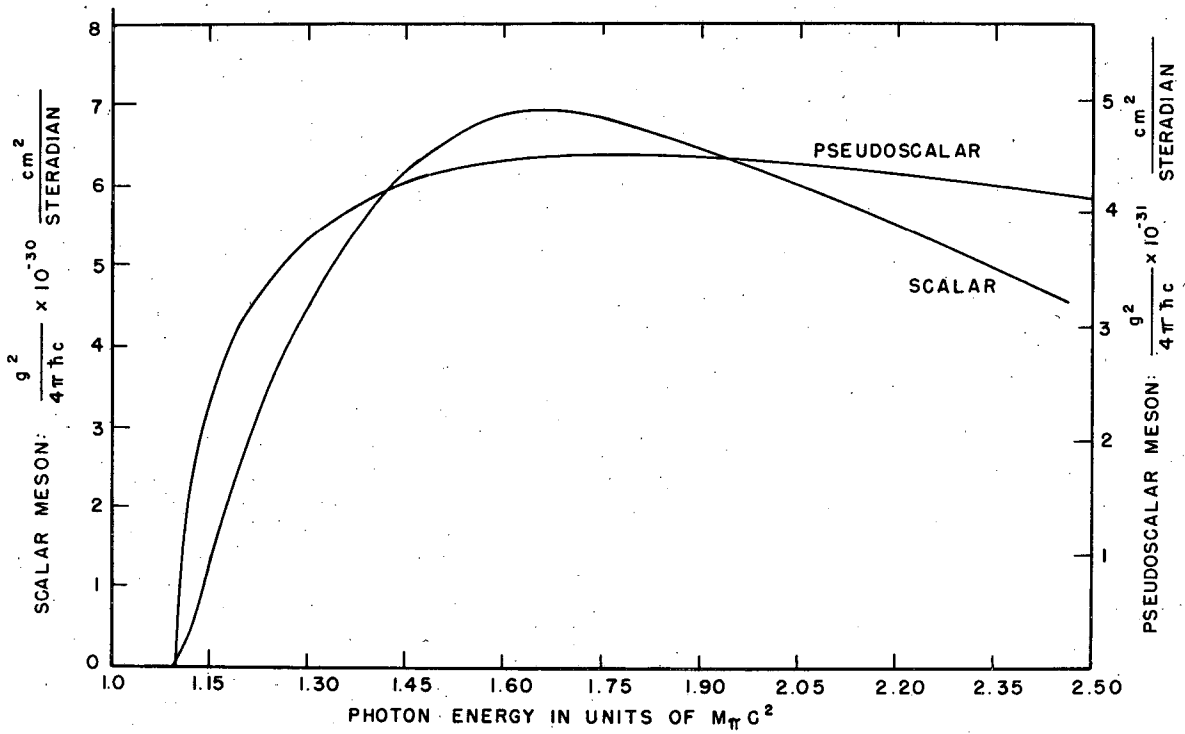
SCALAR MESON: $\frac{g^2}{4\pi\hbar c} \times 10^{-30} \frac{cm^2}{STERADIAN}$
PSEUDOSCALAR MESON: $\frac{g^2}{4\pi\hbar c} \times 10^{-31} \frac{cm^2}{STERADIAN}$
PSEUDOSCALAR
SCALAR
0
1
2
3
4
5
6
7
8
1.0
1.15
1.30
1.45
1.60
1.75
1.90
2.05
2.20
2.35
2.50
PHOTON ENERGY IN UNITS OF $M_\pi C^2$
MU 686

FIG. 21

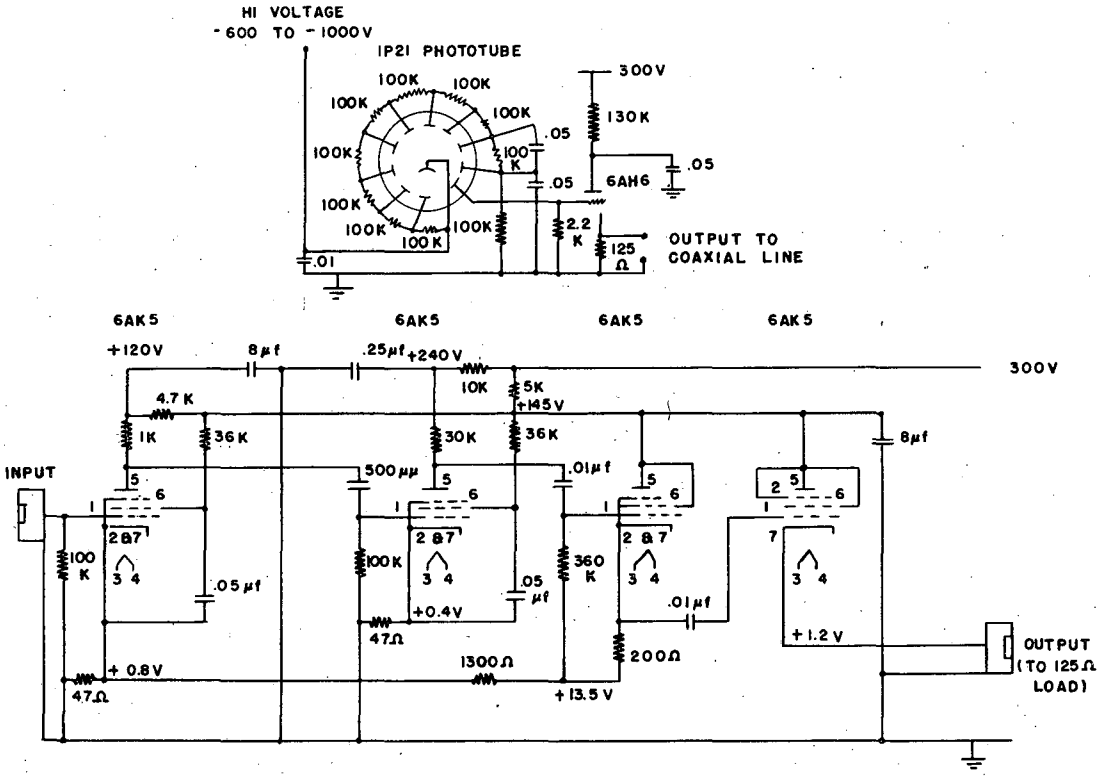

LINEAR AMPLIFIER MU 683

FIG. 22

165131

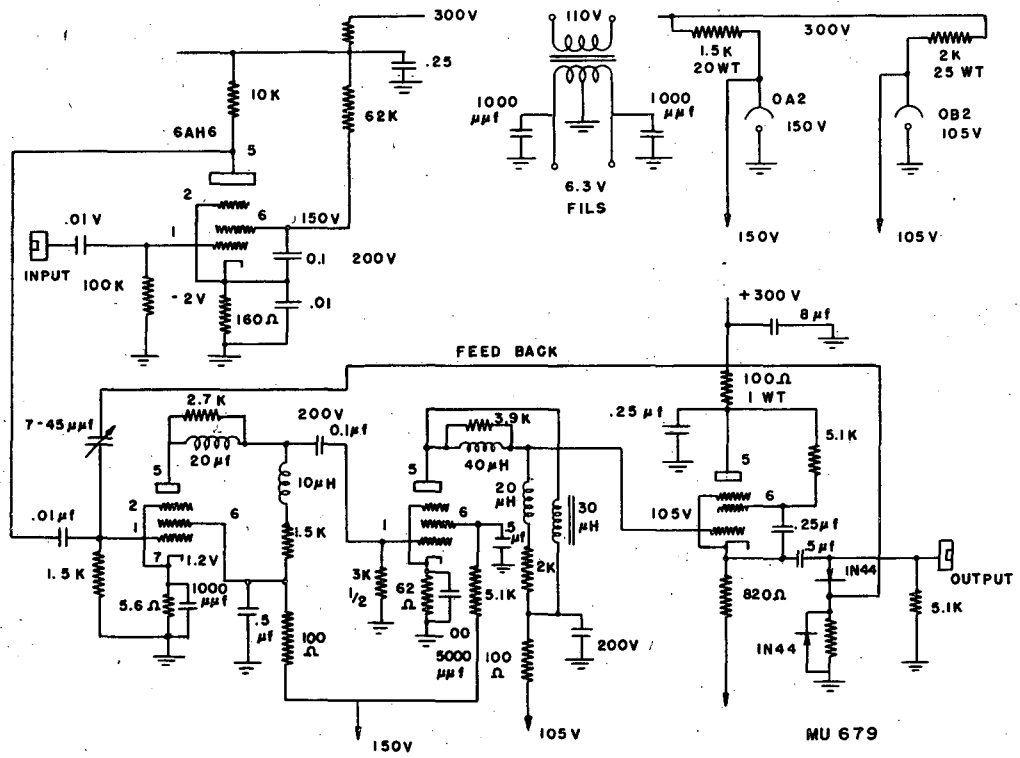

SHAPING CIRCUIT & DISCRIMINATOR
FIG. 23

165061

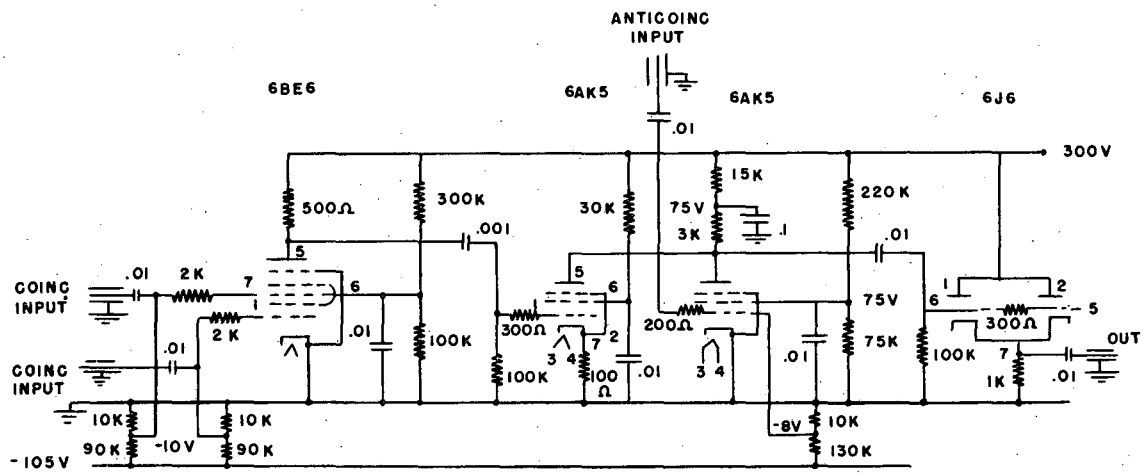

MU 680

COINCIDENCE - ANTICOINCIDENCE CIRCUIT

FIG. 24

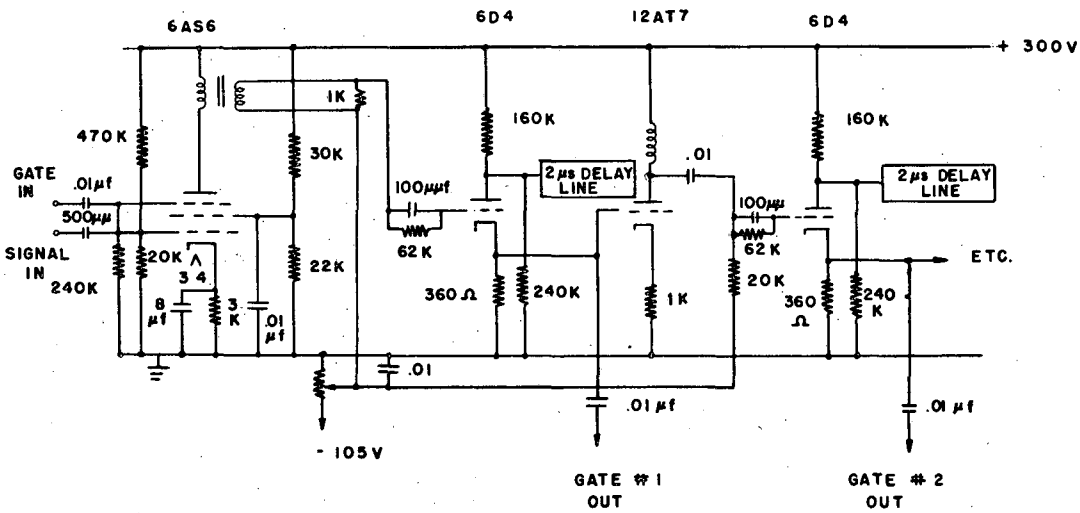

NOTE: THE "GATE IN" CONSTITUTE A LONG (2000 μ sec) GATE BEGINNING JUST BEFORE THE BEAM EMERGES AND ENDING JUST AFTER THE BEAM CEASES. ITS FUNCTION IS TO RENDER THIS CIRCUIT INOPERATIVE EXCEPT WHILE THE BEAM IS STRIKING THE TARGET.

MU 681

FOUR CHANNEL GATE CIRCUIT

FIG. 25

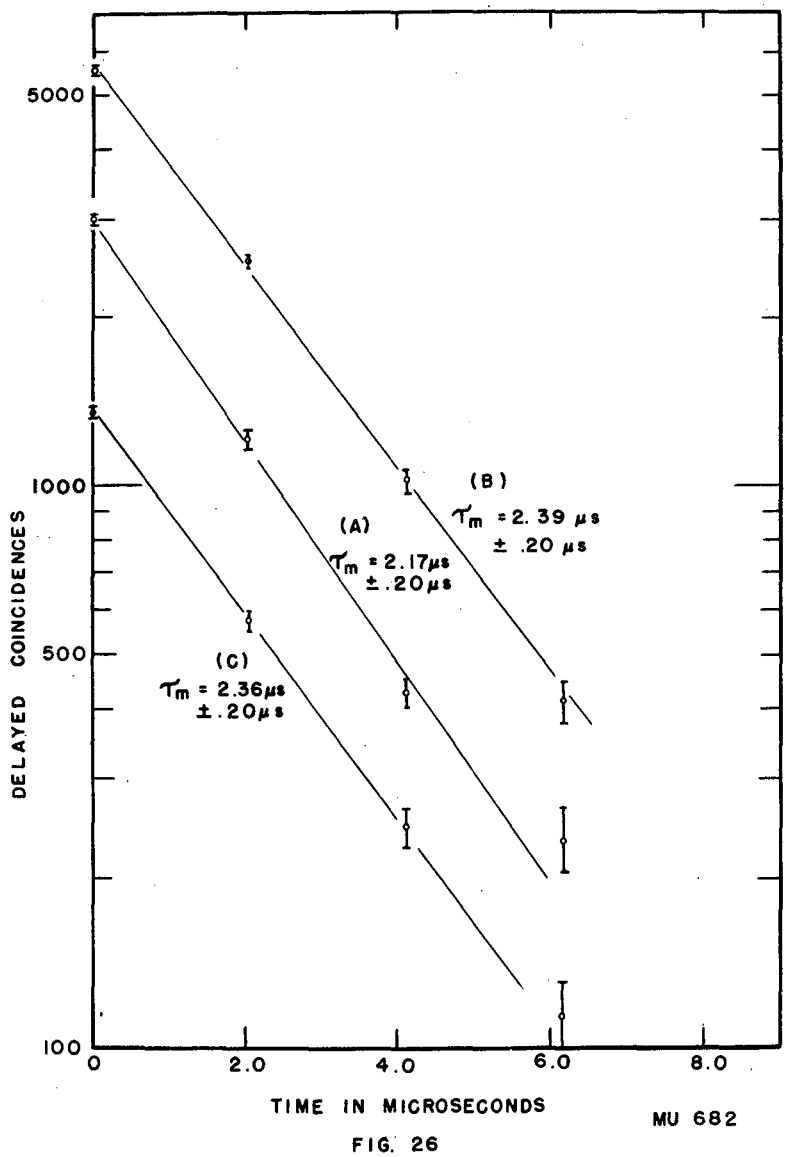
5000
1000
500
100
0
2.0
4.0
6.0
8.0
DELAYED COINCIDENCES
TIME IN MICROSECONDS
(A)
τ_m = 2.17μs
± .20μs
(B)
τ_m = 2.39 μs
± .20 μs
(C)
τ_m = 2.36μs
± .20μs
MU 682

FIG. 26